FIELD TEST PROGRAM OF THE CONCRETE CROSSTIE AND FASTENING SYSTEM

BY

JUSTIN S GRASSE

THESIS

Submitted in partial fulfillment of the requirements
for the degree of Master of Science in Civil Engineering
in the Graduate College of the
University of Illinois at Urbana-Champaign, 2013

Urbana, IL

Adviser:

Professor David A. Lange

ABSTRACT

To adequately satisfy the demands placed on North America's railway infrastructure through ever increasing freight tonnages and development of its high speed rail program, the design and performance of concrete crossties and elastic fastening systems must be upgraded. As a part of a study aimed at improving concrete crossties and fastening systems, field experimentation was performed at the Transportation Technology Center (TTC) in Pueblo, CO by researchers from the University of Illinois at Urbana-Champaign (UIUC). This paper focuses on the transfer of vertical and lateral loads through the system, demonstrating the demands of the fastening components (e.g. insulators, fastening clips) and concrete crossties. Measurements of strain and displacement are provided to quantify the flow of forces through critical interfaces and the physical response of the system under various parameters (track curvature, train speed, car weight, etc.). The data was collected synchronously with measurements of vertical and lateral loads to deterministically track the load path, target areas of uncertainty, and provide validation for a comprehensive finite element model developed by UIUC. Improvements to these instrumentation strategies will also be discussed, as the understanding of the load path and development of the computational model direct the focus to more purposeful measurements for testing to be conducted in May 2013. Finally, the analysis of this data will be used to guide future research in further quantifying the field loading demands, ultimately leading to a mechanistic design approach for the concrete crosstie and fastening system.

ACKNOWLEDGEMENTS

First and foremost, I would like to thank David Lange and Riley Edwards for providing me a great opportunity on this exciting project and for their unrivaled guidance and support ever since. I am also grateful to the many colleagues and friends at UIUC who have made so much of this work possible and enjoyable: Marcus Dersch, Ryan Kernes, Sihang Wei, Chris Rapp, Brandon Van Dyk, George Chen, Jacob Henschen, Daniel Castenada, and Bill Wilson, among many others.

From the railroad industry, I would like to thank Harold Harrison and Mike Tomas for their incomparable expertise; Vince Peterson, Pelle Duong, and George Righter from CXT Concrete Ties, Inc. for providing us time and crossties; Tim Crouch from the Monticello Railway Museum for letting us install ties in our own backyard; and Steve Mattson from VAE Nortrak North America, Inc. for many great discussions. Much of these instruments and tests could not have been done without the help of the Newmark Structural Engineering Laboratory machine shop, including Tim Prunkard, Darold Marrow, and Marc Killion.

Finally I would like to thank all those I love, family and friends, for their invaluable support. Without them none of this would be possible.

Funding for this research effort has been provided by the Federal Railroad Administration (FRA), part of the United States Department of Transportation (US DOT). The published material in this report represents the position of the author and not necessarily that of DOT. This project has also received generous support and guidance from numerous industry partners: Union Pacific Railroad; BNSF Railway; National Railway Passenger Corporation (Amtrak); Amsted RPS / Amsted Rail, Inc.; GIC Ingeniería y Construcción; Hanson Professional Services, Inc.; and CXT Concrete Ties, Inc., an LB Foster Company.

TABLE OF CONTENTS

1. INTRODUCTION

1.1 Background

Historically, in times of increasing freight tonnages and railroad traffic, concrete crossties were used to replace traditional timber crossties. Concrete crossties provide superior durability and capacity, which allow them to outlast standard timber crossties in tracks which have high degrees of curvature and are exposed to extreme weather conditions. [1] Concrete crossties also have the distinct advantage of improved track geometry retention, especially important in sustaining high speed rail and heavy freight lines. [2]

With the continuing increase in annual gross tonnages, concrete crossties are experiencing a wide variety of failure mechanisms. In North America, the most common failure mode is rail seat deterioration (RSD): the wearing out of the concrete within the rail seat, often due to abrasion. [3] In fact, North American Railroads, ranked RSD as the most critical problem facing concrete crosstie track. [4] This abrasion is accelerated in the presence of water and in complex track geometry such as steep track grades and high degree curves. Concrete crossties are also susceptible to flexural cracking, which often propagates from the tie center with diminished ballast support. Other components of the fastening system are also at risk of failure. Fatigue and abrasion of the fastening clips, shoulders, and insulators can allow for additional movement in the system and subsequent deterioration of other components.

In order to understand the mechanisms of the crosstie-fastener system, component behavior and system demands must be investigated. This includes an understanding of load transfer among each component. There is also a need for the magnitude of these input loads with respect to the train speed, car weight, track curvature, grade, and various fastening systems. [5] Obtaining these measurements synchronously will provide insight into the more complex interactions and allow

for a more purposeful, mechanistic design of the system, and the field results to help create more practical design recommendations.

In the pursuit of this mechanistic design, efforts have been made at the University of Illinois at Urbana-Champaign (UIUC) to formulate a comprehensive testing regime that can be implemented in operational track. The instrumentation programs (conducted on July 2012 and May 2013) include the use of strain gauges (surface and embedment), linear potentiometers, and matrix based tactile surface sensors (MBTSS). The full-scale field test will provide measures of vertical and lateral load, rail movement, crosstie displacements, and stresses within the clip and insulator. This data will be investigated with resultant axle loads measured by the Transportation Technology Center, Inc. (TTCI) using an Instrumented Wheelset (IWS).

1.2 Project Objectives

The primary objectives of the field experimentation are to characterize the behavior and quantify the demands placed on each component within the crosstie and fastening system under varying field conditions. The analysis was primarily separated into understanding the vertical and lateral load paths (i.e. the system responses to vertical and lateral loads), although much of the flow of forces cannot be easily decoupled. The load path mapping aids in the process of a mechanistic design of the crosstie-fastener system, which is a design strategy dependent on both analytical and scientific principles. [6] Although it has not been a focus of the railroad industry in recent years, mechanistic design has been a common approach in many other disciplines, including the design of highway pavements. [7] Additionally, this experimentation will provide a means to validate a computational model being developed by the UIUC. This 3-D finite element model will be composed of multiple crossties and a detailed fastening system in order to perform quick parametric analyses (e.g. the effects of fastener types or rail pads on system performance).

Finally, it is also the intent of the program to help facilitate more research in field testing and track system evaluation. The extensive experimental program executed will provide the industry and future researchers insight using industry-accepted approaches as well as novel instrumentation strategies. Significant effort has been made to document the successfulness of each testing program and to make the data accessible to pertinent members of the railroad industry.

2. INSTRUMENTATION PLAN

2.1 Instrumentation Objectives

The overall objective of the field instrumentation is to quantify the demands placed on the crosstie and fastening system components. This data will provide answers to critical questions about the design and performance of concrete crossties and fastening systems, providing a baseline for mechanistic design.

The field measurements will accomplish three primary goals leading to the overall objective:

- **Quantification of Crosstie-Fastener Response** – Instrumentation of the crosstie and fastening system components during testing under known applied loads will lead to a comprehensive understanding of the characteristic deformations of these components.
- **Determination of System Mechanics** – The crosstie and fastener system load transfer mechanics from the wheel-rail interface, through the fastening system, and into the crosstie will be comprehensively understood under known applied loads.
- **Development of Analytical Model** – The data from the field tests will be used in the development of a 3-dimensional finite element model of the crosstie-fastener system that will act as a parametric analysis tool to aid in the design of concrete crossties and fastening systems.

2.2 Overview of Field Test

In July 2012, two sections of track were investigated at the Transportation Technology Center (TTC) in Pueblo, CO. One section was on tangent track while the other was on curved track with a curvature of about 5°. For both sections, 15 new concrete crossties were installed with

new ballast, sufficiently tamped, and exposed to approximately 5MGT of freight traffic prior to testing. The loading environment consisted of a passenger consist, freight consist, and a Track Loading Vehicle (TLV) for static loading. A description of the test program is outlined in Appendix B.

A large set of measurements were conducted on three adjacent rail seats and the opposite rail seat of the center tie (labelled orange in Figure 3). Additional rail seats in the section will be partially instrumented with vertical strain gages on the rail. The measurements recorded during the field instrumentation along with their locations are included in Table 1. This table also includes the reference section, the rail seat locations that were tested and the test sections at which these measurements are implemented.

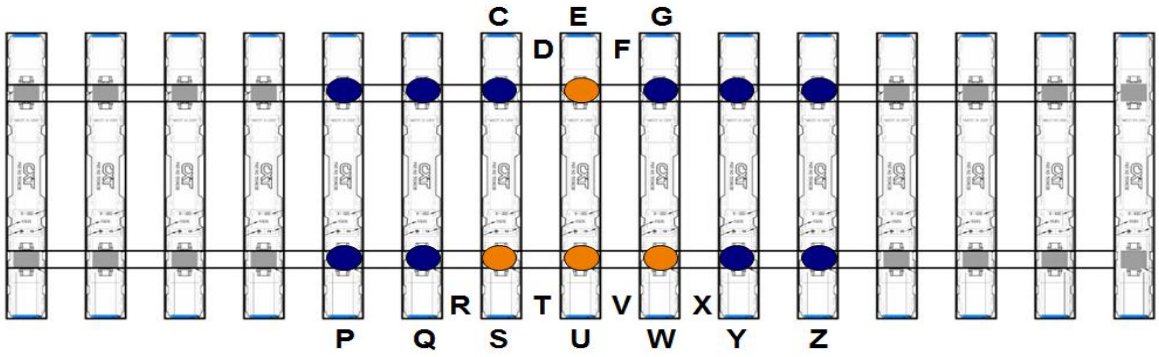

Figure 1: Locations of fully (orange) and partially (blue) instrumented rail seats.

Table 1: Measurements recorded in July 2012 Field Instrumentation with locations.

Measurement Type	Reference Section	Rail Seat Locations
Vertical wheel loads	3.5.1	D, F, T, V
Vertical rail seat loads	3.5.2	E, S, U, W
Lateral wheel loads	3.5.3	E, S, U, W
Vertical rail base displacements	3.5.4	E, S, U, W
Lateral rail displacements	3.5.5	E, S, U, W
Vertical crosstie displacements	3.5.6	Ties C/S, E/U, G/W
Internal crosstie strains	3.5.7	E, S, U, W
External crosstie strains	3.5.8	Ties C/S, E/U, G/W
Rail seat pressure distributions	3.5.9	G, W, Y
Rail base bending stresses	3.5.10	E, S, U, W
Insulator post stresses	3.5.11	E, S, U, W
Fastening clip stresses	3.5.12	E, S, U, W
Vertical rail strains	3.5.13	ALL

Additional wheel load measurements were taken by our partners at TTC using an Instrumented Wheel set (IWS). These results were used in verifying the range of input loads measured and supplemented the data analysis.

2.3 Summary of Test Measurements

Many measurements were taken to accomplish the objectives outlined above. Some measurements were collected using well established instrumentation methodologies, while others used novel approaches.

The following is a list of all the measurements that were taken in the July 2012 instrumentation plan and a description of how they were measured. For these descriptions the following naming convention for the orientation of principal axes related to the test set up is included below (see Figure 2):

X – Transverse direction of the track

Y – Vertical direction (gravity)

Z – Longitudinal direction of the track

Figure 2: Naming convention of principal axes.

2.3.1 Vertical Wheel Loads

Vertical wheel loads was determined using an arrangement of strain gages in the crib of the rail (Figure 3). Weldable strain gages will be assembled in a Wheatstone bridge and calibrated with a TLV. Gages are placed in the chevron pattern (Figure 3) about the neutral axis of the rail section as shown, oriented at 45° to the neutral axis. Four gages are mirrored on each side of the rail. The centers of the two groups of gages are measured at 5" from each side of the center of the crib. This has served as a commonly used methodology for determining accurate measurements

of vertical wheel loads, well established within the railroad industry since its development in the 1970's. [8]

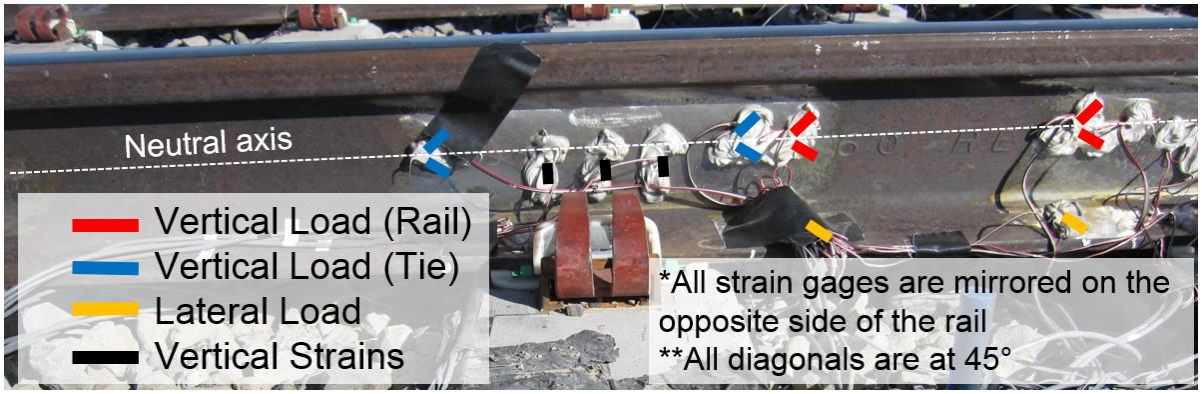

Figure 3: Strain gage configurations for load circuits.

The vertical load, P_Z, can be determined by:

$$P_Z = V_{ZL} - V_{ZR} \tag{1}$$

The shear forces at each face (V_{ZL} and V_{ZR}) can be calculated as follows:

$$V_{ZL} = \frac{EI}{(1+\nu)Q}\varepsilon_1 \tag{2}$$

$$V_{ZR} = \frac{EI}{(1+\nu)Q}\varepsilon_2 \tag{3}$$

where E is the steel modulus of elasticity, I is the the moment of inertia of the rail cross-section, ν is the Poisson's ratio, Q is static moment of area, and the principal strains (ε_1 and ε_2) are comprised of the strains shown in Figure 4:

$$\varepsilon_1 = \varepsilon_a - \varepsilon_b + \varepsilon_{a'} - \varepsilon_{b'} \tag{4}$$

$$\varepsilon_2 = \varepsilon_c - \varepsilon_d + \varepsilon_{c'} - \varepsilon_{d'} \tag{5}$$

Thus, the load P_z could be rewritten as:

$$P_Z = \frac{EI}{(1+\nu)Q}(\varepsilon_1 - \varepsilon_2) \tag{6}$$

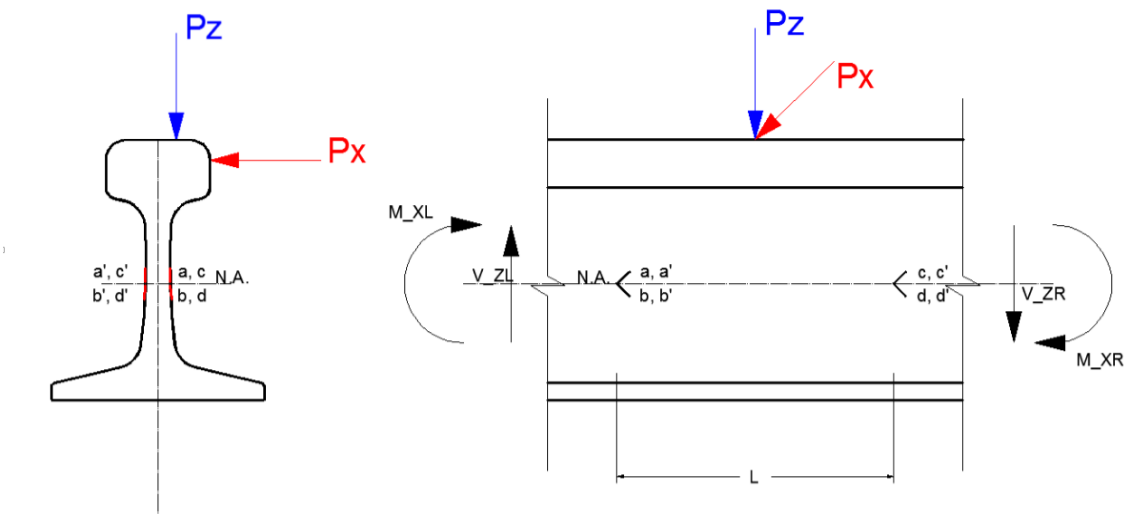

Figure 4: Vertical applied load and strain gage diagram.

The strains ε_1 *and* ε_2 can be obtained by using a Wheatstone bridge (Figure 5). Strain ε_1 can be measured separately by using the Wheatstone bridge connection shown on the left of Figure 5, and strain ε_2 can be found similarly. The strain difference $(\varepsilon_1 - \varepsilon_2)$ can then be measured directly by including each strain gage into the Wheatstone bridge connection shown on the right of Figure 5.

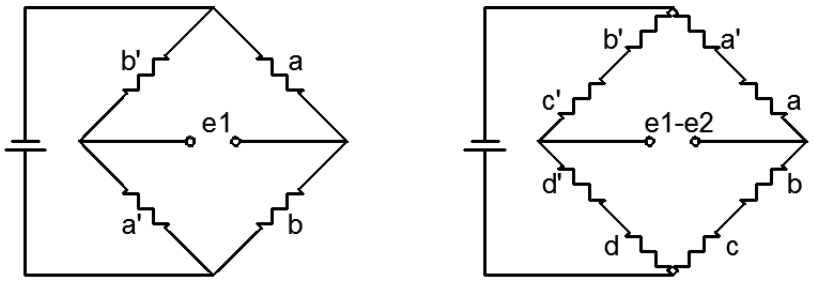

Figure 5: Wheatstone bridge connections.

2.3.1.1 Calibration

A TLV owned by the Association of American Railroads (AAR), equipped with actuators and load cells was used for the calibration of both the vertical and lateral load gage patterns. The calibration was conducted as follows for all full-bridge circuits:

1. The TLV deployable axle was positioned above the center of the crib with the strain gauge assembly.
2. Output was recorded from the vertical load circuit (2.3.1).
3. Vertical loads were applied in increments of 5 kips, until a maximum of 40 kips was reached.
4. The gain factor was recorded for the vertical load strain gage bridges, using measurements of each vertical load step.
5. Output was recorded from the lateral load circuit (2.3.3).
6. Increments of 2 kip lateral load were then applied, while sustaining the vertical load, until a maximum of 20 kips lateral load.
7. The gain factor was recorded for the lateral load strain gage bridges, using measurements of each lateral load step.

Figure 6: Track Loading Vehicle (TLV) in operation.

2.3.2 Vertical Rail Seat Loads

Vertical rail seat loads were determined using the same arrangement of strain gages on the rail web as in section 2.3.1, but directly above the rail seat (Figure 3). Weldable strain gages were assembled in a Wheatstone bridge and the calibration from section 3.2.1 was used to capture the shear difference across this circuit. The rail seat forces (loads transferred into the crosstie) were determined by taking the difference of this measurement and an adjacent vertical wheel load measured in the crib.

2.3.3 Lateral Wheel Loads

Lateral wheel loads were determined using an arrangement of strain gages in the crib of the rail (Figure 3). Instead of measuring shear in the y-direction, these shear strains were rotated about x-axis and positioned on the rail base in order to measure shear in the direction of the lateral loads. Weldable strain gages were assembled in a Wheatstone bridge, similar to the left diagram in Figure 5, and calibrated with the TLV (2.3.1.1).

2.3.4 Lateral Rail Displacements

Lateral rail displacements were measured at the rail base and the neutral axis of the rail relative to the crosstie using linear potentiometers. These measurements captured the lateral movement and stiffness of the system. The potentiometers used to measure lateral displacements were screwed onto a small aluminum plate epoxied to the crosstie (Figure 7). Two points were measured (one at the base and one at the neutral axis, Figure 8, left) to determine average lateral displacement as well as rotation and bending of the rail, about the z-direction.

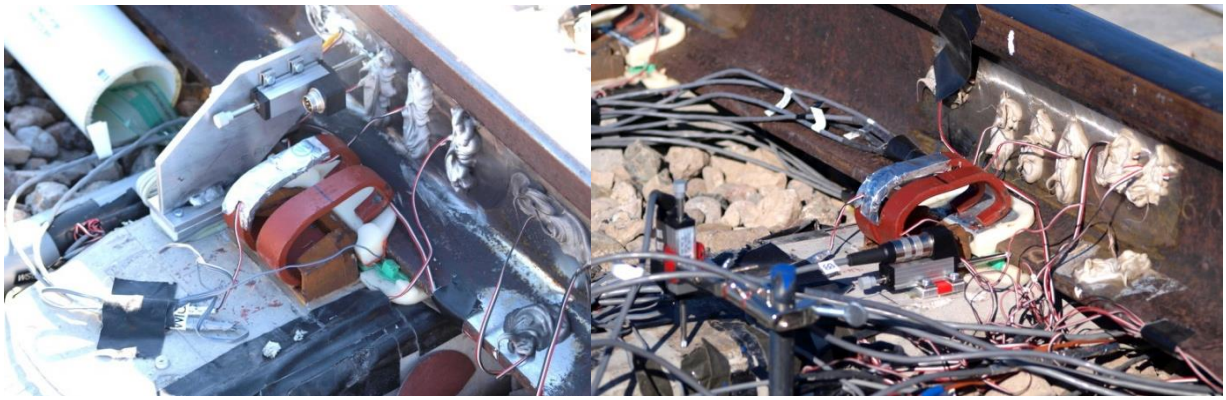

Figure 7: Position of linear potentiometer on the rail web (left) and rail base (right).

2.3.5 Global Vertical Crosstie Displacements

Global vertical displacements of the crosstie were measured with linear potentiometers affixed to 6' rods driven into the subgrade. These measurements were taken at the two ends of a crosstie (seen in the forefront of the right picture in Figure 7). These measurements captured the local stiffness of the substructure. Additionally, they provided a representation of the rigid body movement (uniform and differential compression of the substructure).

2.3.6 Internal Crossties Strains

Internal crosstie strains were measured 1.5" below the surface of the rail seat using embedment gages (Figure 8). Embedment gages were installed during crosstie manufacturing in a 2x2 pattern (centered and spaced 3" apart). These strains have been used to investigate relative rail seat loads (using average strain values) and rail seat stress distributions. Much of the data from the July 2012 testing has been post-processed and looks promising. The analysis of these measurements is still being carried out by Sihang Wei (UIUC) and is not covered in this paper.

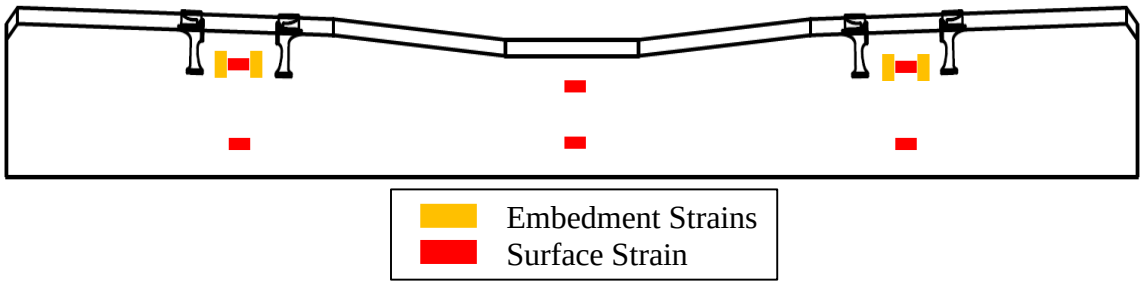

Figure 8: Crosstie strain gage locations.

2.3.7 External Crossties Strains

External crosstie strains were determined by concrete surface strain gages positioned longitudinally to the crosstie below the rail seats and tie center (Figure 8). Knowing the distance between these strains provides a measurement of curvature and, provided the cross-sectional properties of the crosstie, bending moments at three integral sections. Similar to the embedment gages, the data analysis of these strains is ongoing with the work of Sihang Wei (UIUC) and is discussed within section 4.3.2.

2.3.8 Rail Base Bending Stresses

Rail base bending stresses were determined using weldable strain gages 1” from the edge of the field-side rail base in the x-direction (Figure 9). These strains demonstrate the magnitude of bending of the rail base. This helps to assess the mechanistic behavior of the rail (i.e. the proportion of the rail base that is attributable to bending of the flange, opposed to rigid body rotation). There is limited discussion regarding this methodology within this paper, but plots are included in Appendix A.

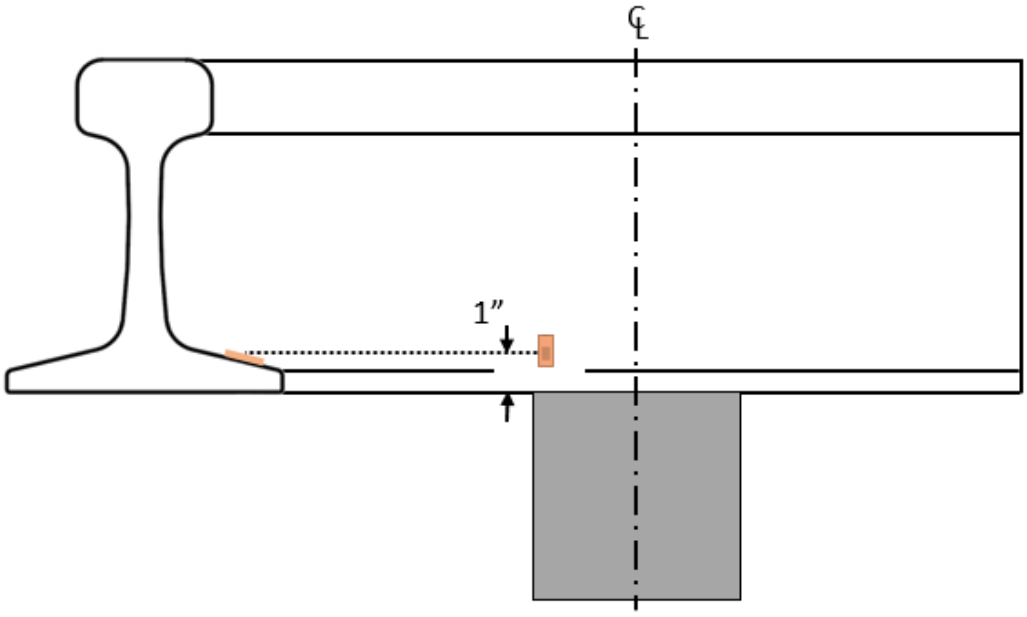

Figure 9: Location of transverse gages to measure rail base bending stresses.

2.3.9 Fastening Clip Stresses

Fastening clip stresses were determined using strain gages on the surface of fastening clips on both the field and gauge side of the rail in the x-direction. This strain value has provided, with coordination with the computational modelling work, an indicator of clamping force and loading demands on each fastening clips.

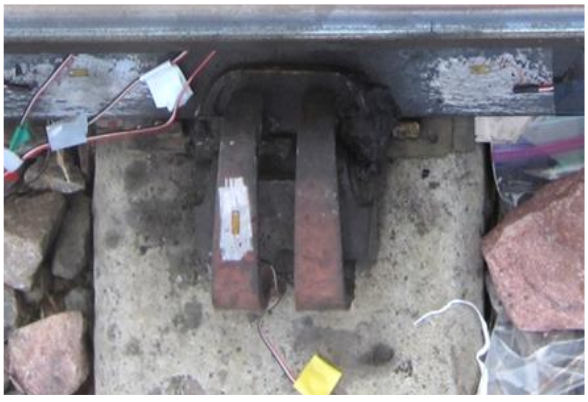

Figure 10: Location of strain gage on fastening clip.

2.3.10 Vertical Rail Strains

Vertical rail strains were measured near the base of the web (Figure 3). Three vertical strain gages were centered 2” apart on each side of the rail, 2” above the rail base (Figure 11). These strains demonstrated the stress behavior of the rail along a stretch of seven crossties, as well as strain inputs for the validation of the finite element model. Measured across seven crossties, these strains were used to assess vertical and lateral load distribution in both static and dynamic cases.

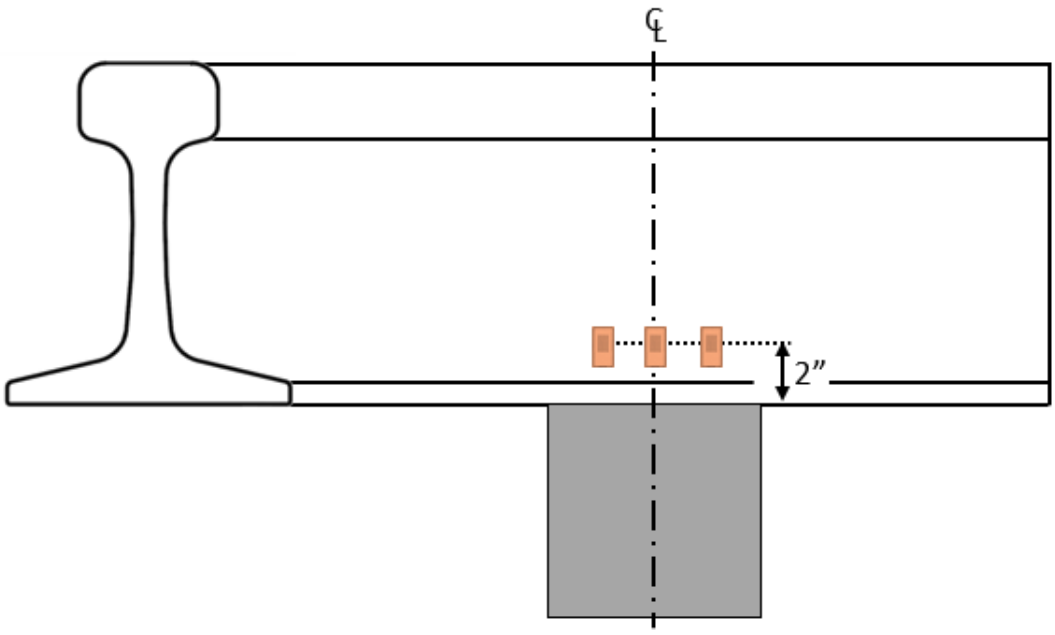

Figure 11: Locations of vertical strain gages above rail seat.

2.3.11 Rail Seat Pressure Distribution

The distribution of pressure on the rail seat areas was determined using MBTSS. These sensors were able to map the distribution of loads onto a single rail seat surface, however, the sensors were first calibrated by applying known loads with a vertical loading frame and using input loads calculated through the strain gage data. MBTSS was installed on both rail seats of the

crosstie about which full instrumentation of strain gauging took place, with the purpose of measuring the distribution of the load onto the concrete rail seat surface. Data was collected from both rail seats simultaneously during various periods of train operation. A single rail seat on an adjacent crosstie was also instrumented with MBTSS, in order to collect data from successive crosstie rail seats during train operation.

Installing the sensors involved removing the fastening clips of the crossties to be instrumented, as well as approximately five crossties on either side to raise the rail to a height adequate for accurately placing a sensor. The rail was then lowered and all the clips reapplied. Removal of the sensors required the same process. Figure 12 shows a profile view of the fully instrumented crosstie with all components of the MBTSS installation. Figure 13 shows a plan view of the MBTSS as it was installed on the rail seats.

Although there has been extensive data analysis of laboratory studies with MBTSS, much of the data analysis from the July field test is on-going by Christopher Rapp (UIUC). Therefore there is limited discussion regarding this methodology within this paper, but data is included in Appendix A.

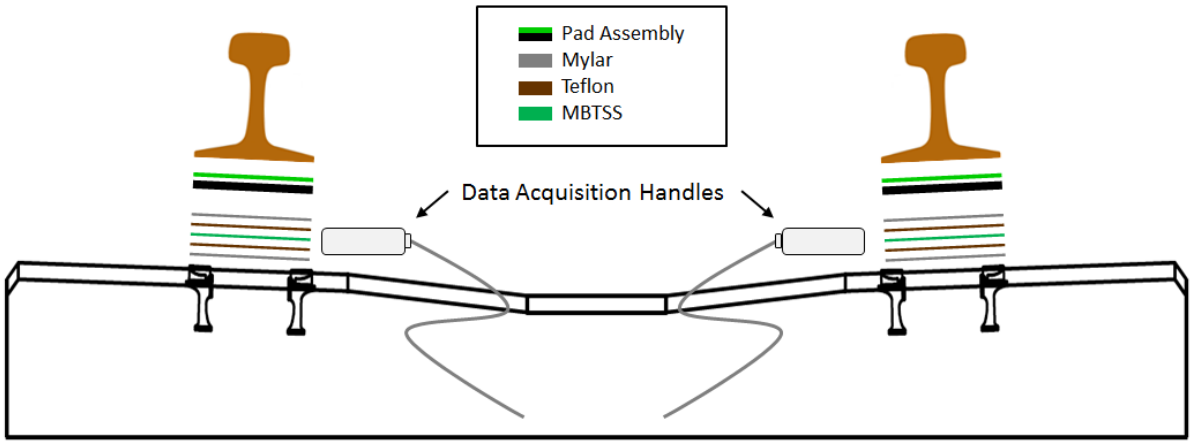

Figure 12: Profile view of MBTSS installation on crosstie.

Figure 13: Plan view of MBTSS installation on crosstie.

3. FIELD DATA

This section includes figures of the data accumulated from the July 2012 Field Instrumentation Program at TTC. These results include measured loads, displacements, rail strains, and fastening clip strains. Additional figures can be found in the attached **Appendix A**.

3.1 Loads

Figure 14 shows the distribution of vertical wheel loads from a freight consist on tangent track. Each section includes the vertical loads imparted by each axle of a 9-car freight consist at various speeds (15-60mph) separated into quartiles.

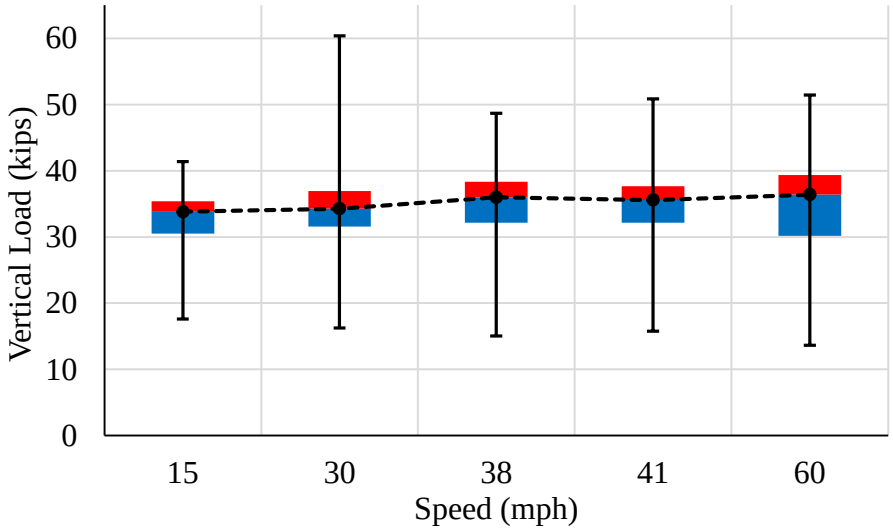

Figure 14: Vertical wheel loads imparted by a freight consist on tangent track.

Figure 15 shows the distribution of vertical wheel loads from a freight consist on curved track (high and low rail). Each section includes the vertical loads imparted by each axle of a 9-car freight consist at various train speeds (15, 30, and 45mph) separated into quartiles.

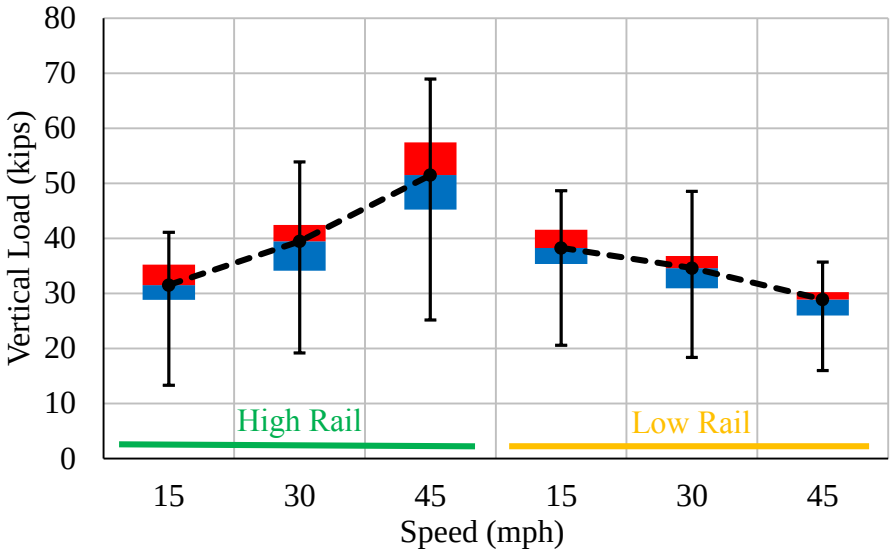

Figure 15: Vertical wheel loads imparted by a freight consist on curved track.

Figure 16 shows the distribution of vertical wheel loads from a passenger consist on tangent track. Each section includes the vertical loads imparted by each axle of a 9-car passenger consist (excluding the locomotive) at various speeds (15-102mph) separated into quartiles.

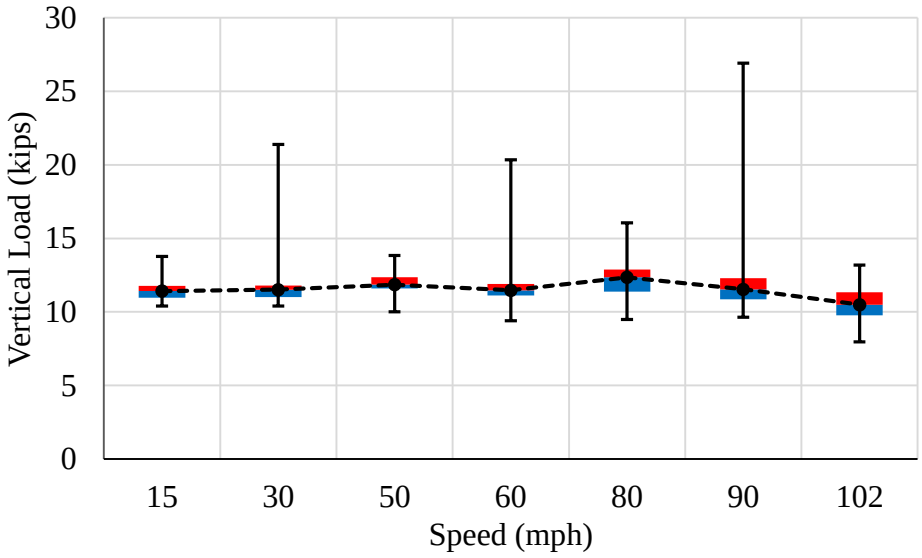

Figure 16: Vertical wheel loads imparted by a passenger consist on tangent track.

Figure 17 shows the distribution of rail seat loads from a freight consist on tangent track. Each section includes the rail seat loads imparted by each axle of a 9-car freight consist at various speeds (15-60mph) separated into quartiles.

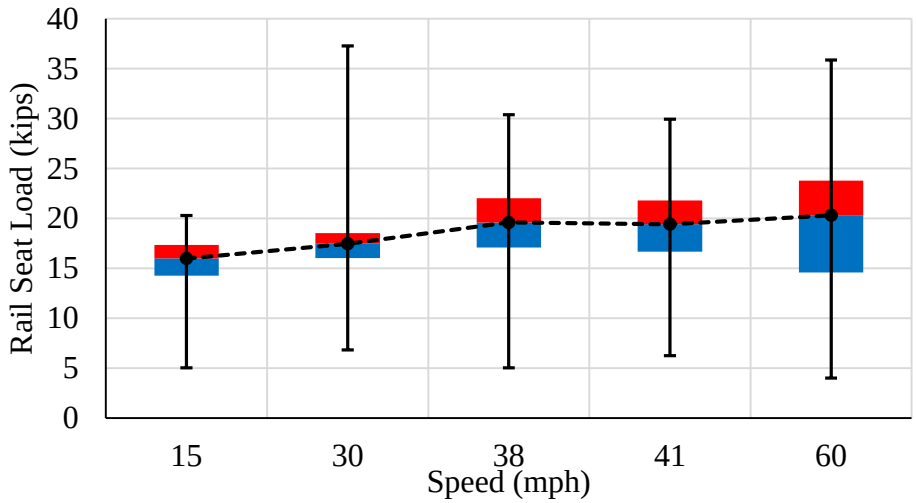

Figure 17: Rail seat loads imparted by a freight consist on tangent track.

Figure 18 shows the distribution of rail seat loads from a passenger consist on tangent track. Each section includes the rail seat loads imparted by each axle of a 9-car passenger consist at various speeds (15-102mph) separated into quartiles.

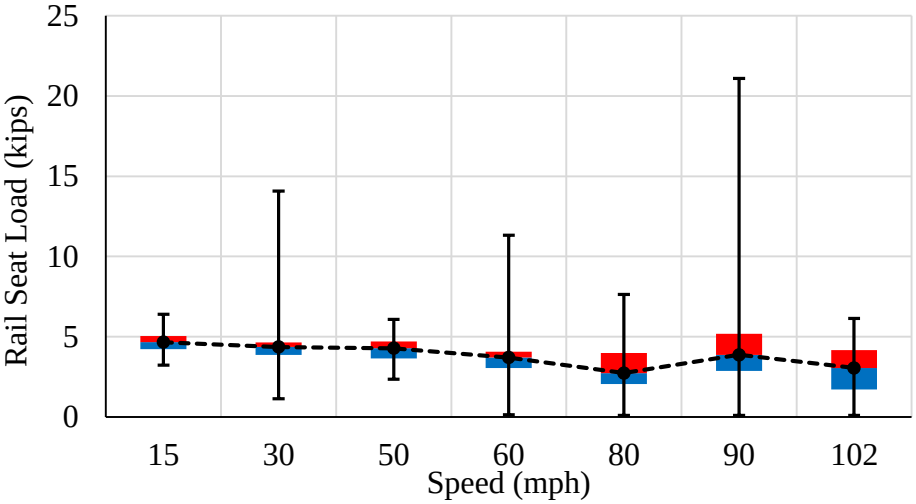

Figure 18: Rail seat loads imparted by a passenger consist on tangent track.

Figure 19 shows the distribution of lateral wheel loads from a freight consist on tangent track. Each section includes the lateral loads imparted by each axle of a 9-car freight consist at various speeds (15-60mph) separated into quartiles.

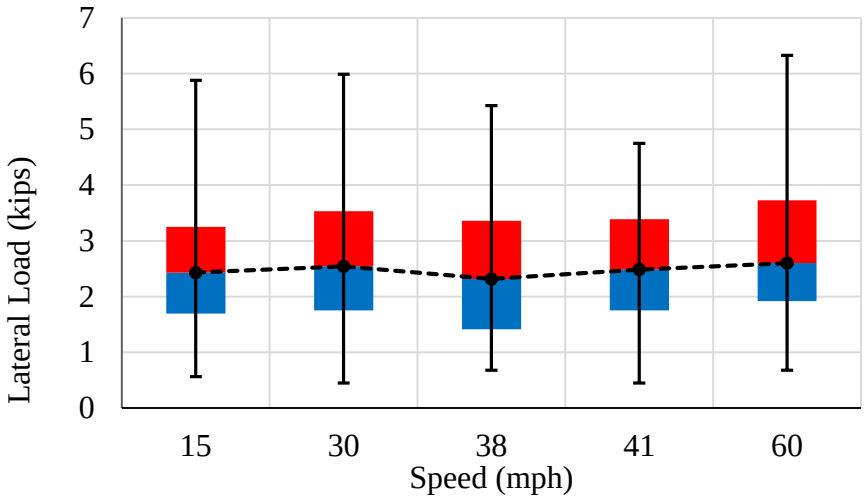

Figure 19: Lateral wheel loads imparted by a freight consist on tangent track.

Figure 20 shows the distribution of lateral wheel loads from a 9-car freight consist imparted on the high rail of a curved track. Each section includes the lateral loads imparted by each axle of the freight consist at various speeds (2-41mph) separated into quartiles.

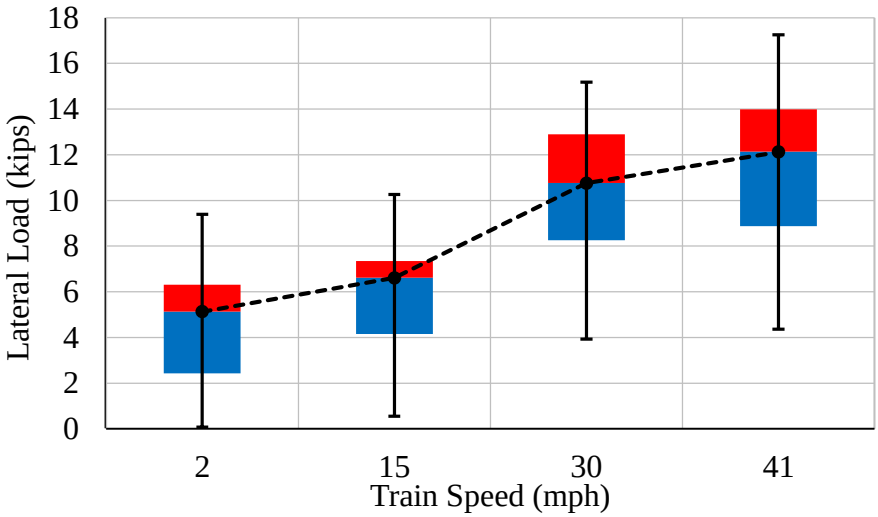

Figure 20: Lateral wheel loads imparted by a freight consist on the high rail of curved track.

Figure 21 shows the distribution of lateral wheel loads from a 9-car freight consist imparted on the high rail of a curved track. Each section includes the lateral loads imparted by each axle of the freight consist at various speeds (2-41mph) separated into quartiles.

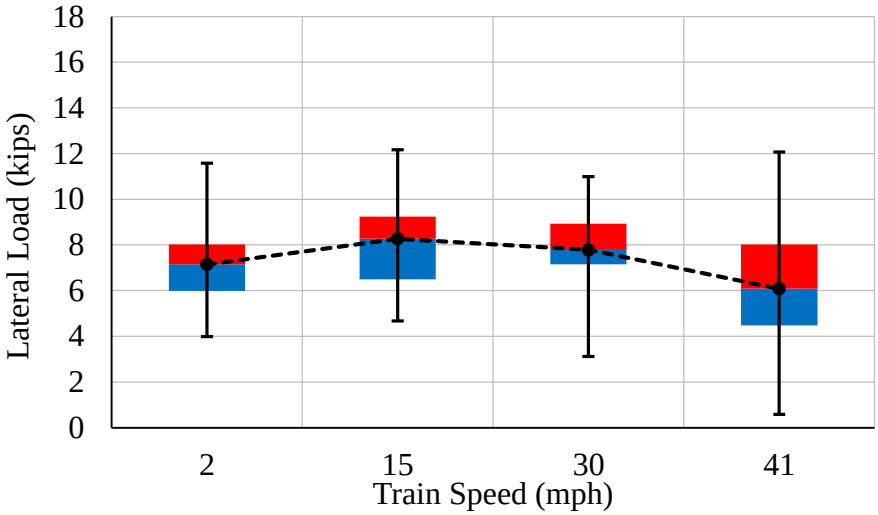

Figure 21: Lateral wheel loads imparted by a freight consist on the low rail of curved track.

Figure 22 shows the distribution of concurrent lateral and vertical axle loads. Each point represents an axle load (the vertical and lateral components) from a freight train on tangent track at 15 and 60mph.

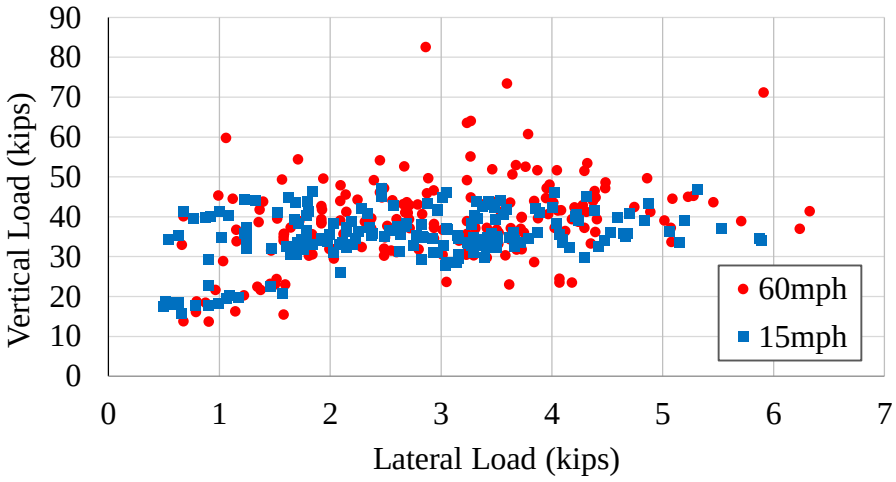

Figure 22: Vertical and lateral wheel loads from a freight consist on tangent track.

Figure 23 shows the distribution of concurrent lateral and vertical axle loads. Each point represents an axle load (the vertical and lateral components) from a freight train on the high rail of a curved track at 15, 30 and 45mph. This plot also includes trendlines of these distributions.

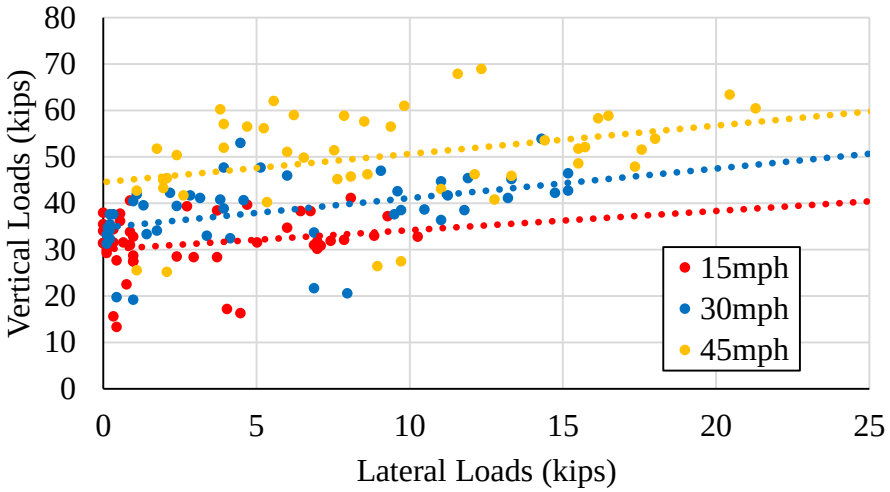

Figure 23: Vertical and lateral axle loads from a freight consist on the high rail of curved track.

Figure 24 shows the distribution of concurrent lateral and vertical axle loads. Each point represents an axle load (the vertical and lateral components) from a freight train on the low rail of a curved track at 15, 30 and 45mph. This plot also includes trendlines of these distributions.

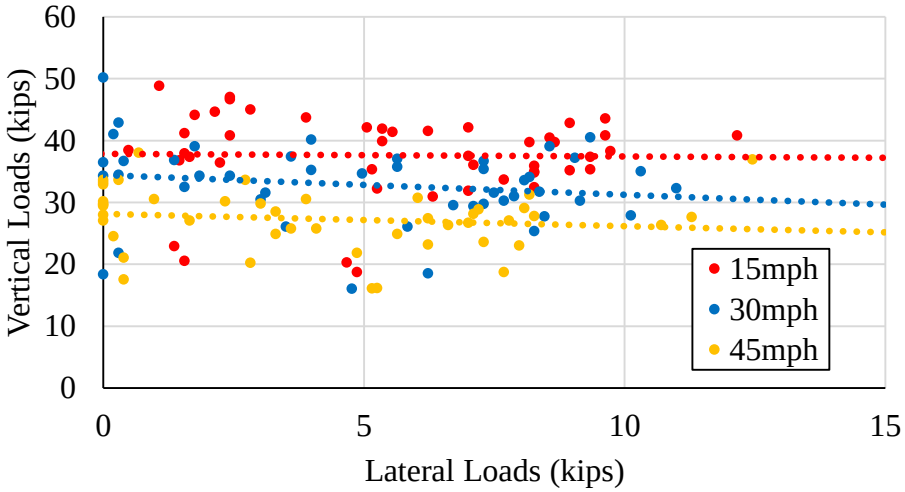

Figure 24: Vertical and lateral axle loads from a freight consist on the low rail of curved track.

Figure 25 shows the correlation between concurrent lateral and vertical loads acting on curved track from a freight consist at various speeds (15, 30, 45mph). The loads are denoted in bold lines labelled "HR" for the high rail and "LR" for the low rail.

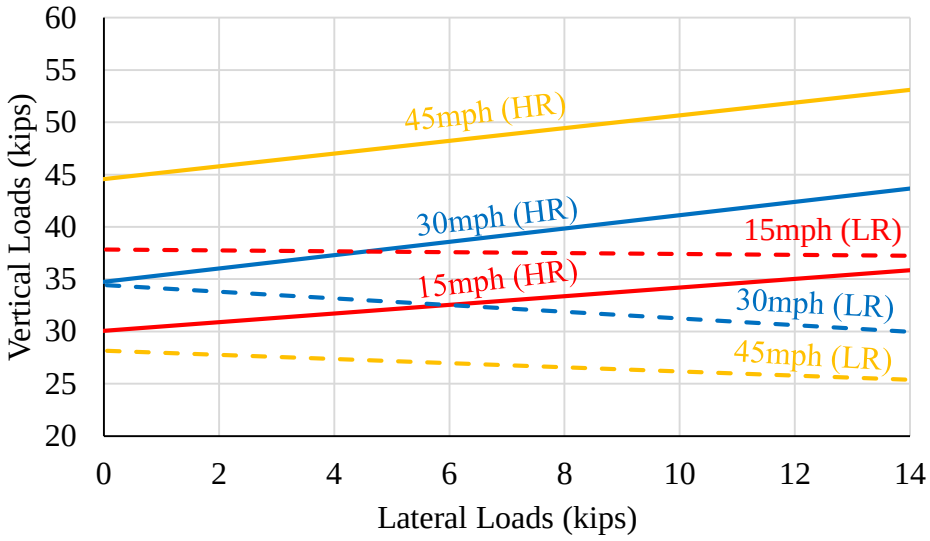

Figure 25: Correlation between lateral and vertical axle loads on curved track.

Figure 26 shows the average vertical load being transferred into the rail seat as a percentage of the vertical wheel load imparted by a freight consist on tangent track. This plot includes load transfers of multiple rail seats at various train speeds (2-60mph).

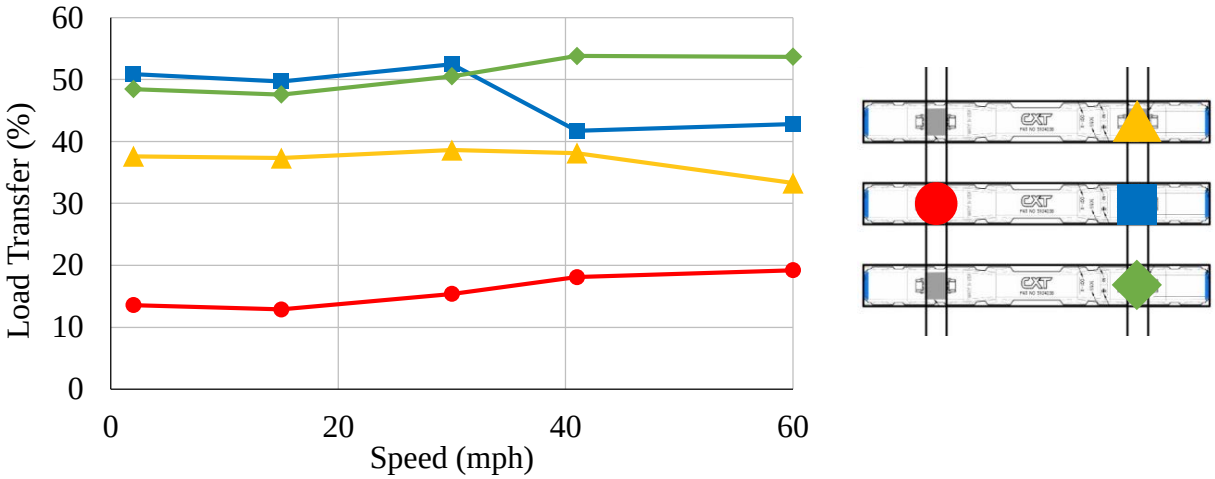

Figure 26: Percentage of load being transferred into the crosstie

Figure 27 shows vertical crossties displacements and associated rail seat loads of three rail seats being loaded vertically by the TLV at each respective rail seat. Each marker represents an increment of 5kips of vertical load (a maximum of 40kips).

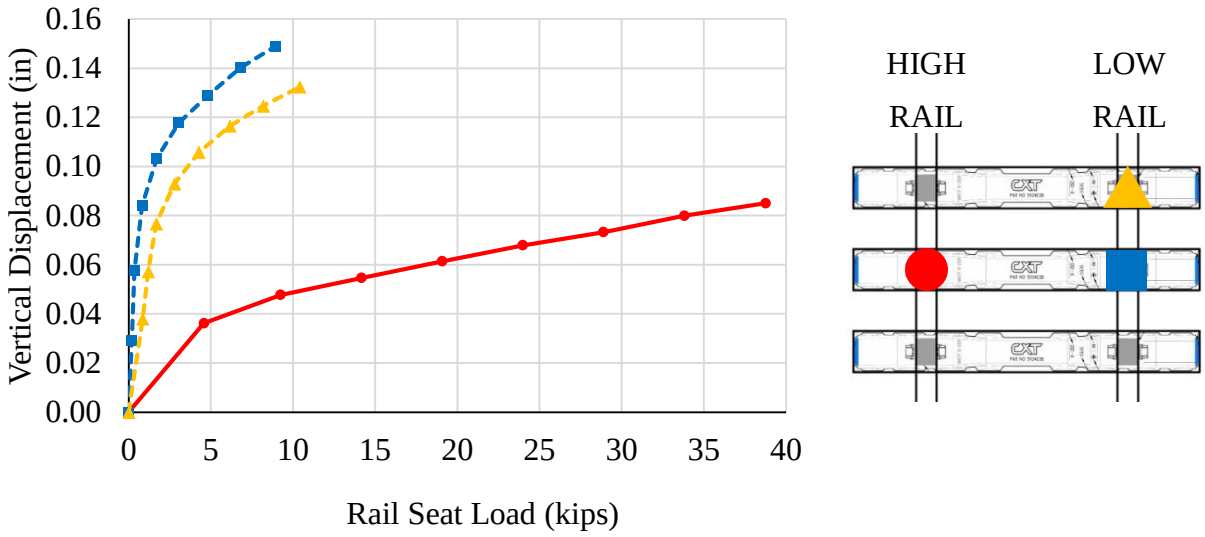

Figure 27: Vertical crosstie displacements and rail seat loads from static vertical loading.

Figure 28 shows average vertical wheel loads and rail seat loads imparted by a freight consist on curve track. The plot includes measurements of the high rail (HR) and low rail (LR).

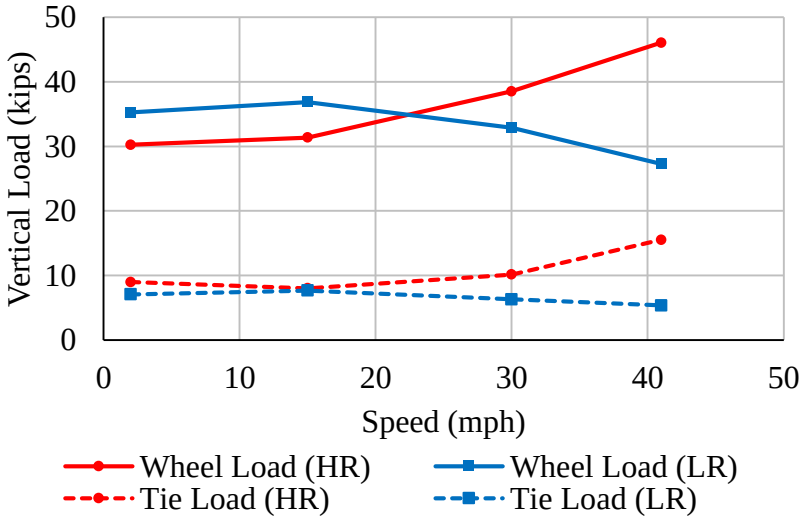

Figure 28: Average vertical wheel and rail seat loads imparted by a freight consist on a curve.

3.2 Displacements

Figure 29 shows vertical crosstie displacements at the ends of three adjacent crossties with a static vertical load being applied at the center crosstie. Each marker represents a static vertical load of 5kips (maximum of 40kips) applied by the TLV.

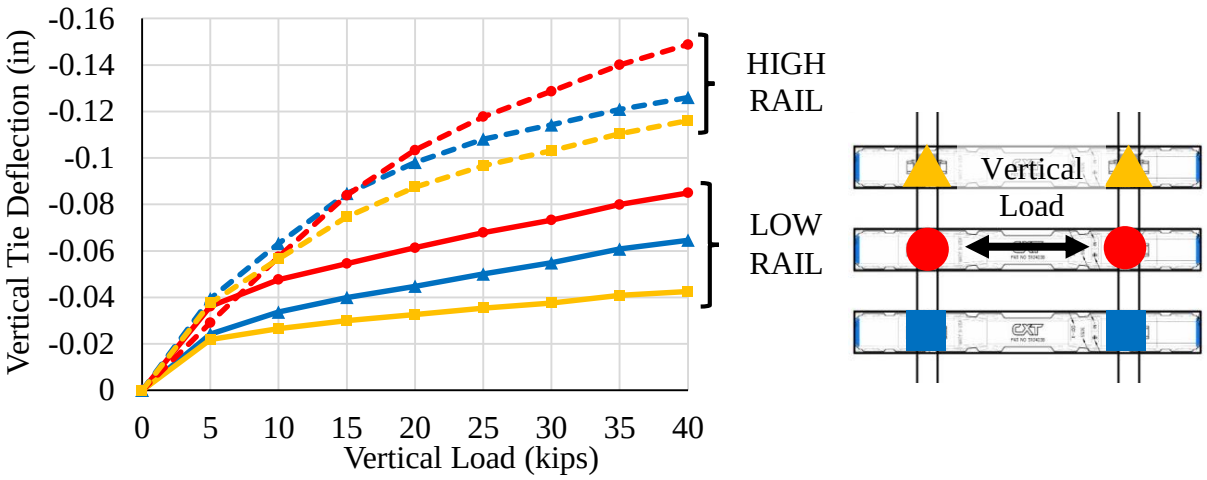

Figure 29: Vertical crosstie displacements of adjacent rail seats from static vertical loads.

Figure 30 shows vertical crosstie displacements at the ends of three adjacent crossties with a static vertical load of 40kips being applied at the first crosstie by the TLV.

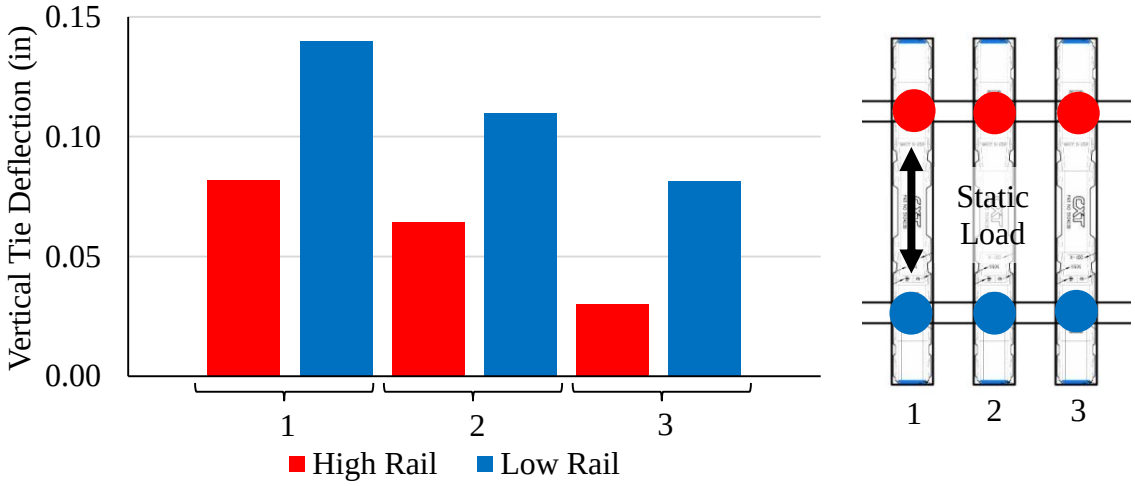

Figure 30: Vertical deflections of adjacent crossties under static loading.

Figure 31 shows vertical crosstie displacements and associated vertical loads from axles on a freight and passenger consist on tangent track. The markers represent the responses to each axle of six train passes at 15, 30, and 60mph. The solid line represents the static deflection from vertical loads applied by the TLV, with the dotted lines representing fractions of that static deflection.

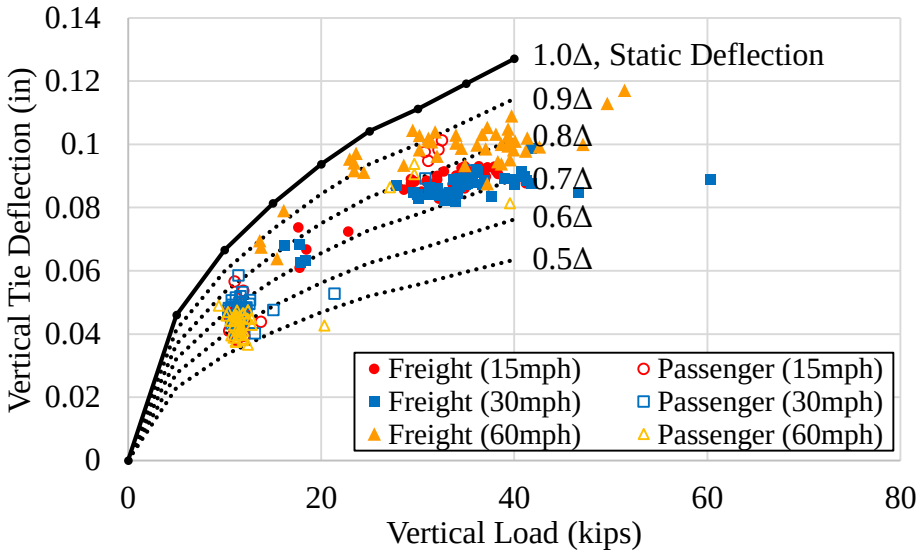

Figure 31: Vertical crosstie displacements of passenger and freight consists

Figure 32 shows outward lateral displacements of the rail web (red) and base (blue) over a rail seat on the low rail of a curve. The solid lines represent static responses as measured from 20kips of static lateral load being applied by the TLV, with a constant 40kips of vertical load. The additional points represent responses taken from each axle of a freight consist going over the low rail of a curve at 2mph.

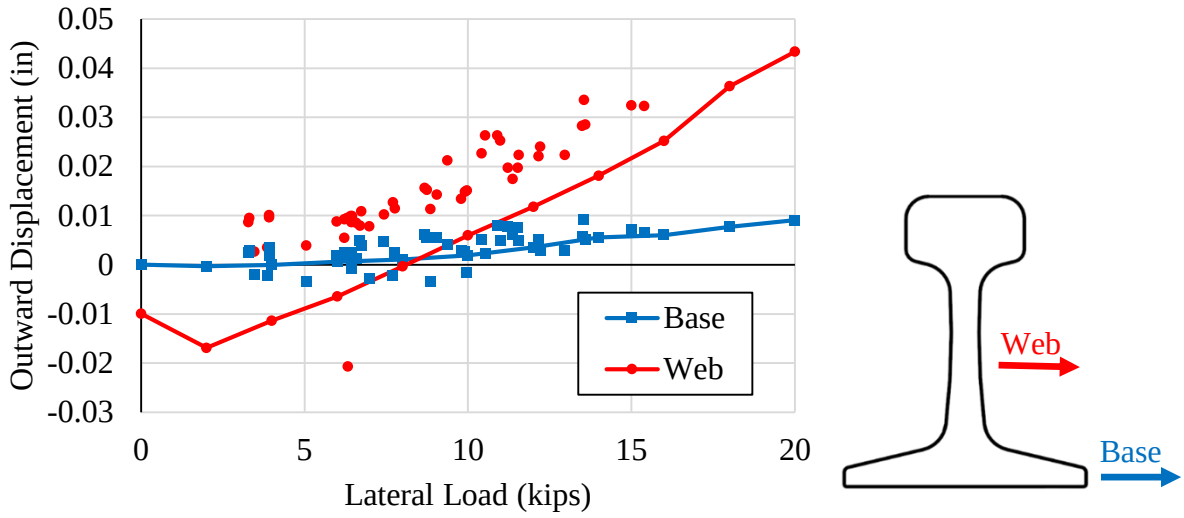

Figure 32: Lateral displacements of the low rail from static and dynamic lateral loads.

Figure 33 shows outward lateral displacements of the rail web and base over a rail seat on the high rail of a curve. The solid lines represent static responses as measured from 20kips of static lateral load being applied by the TLV, with a constant 40kips of vertical load. The additional points represent responses taken from each axle of a freight consist over the high rail of a curve at 2mph.

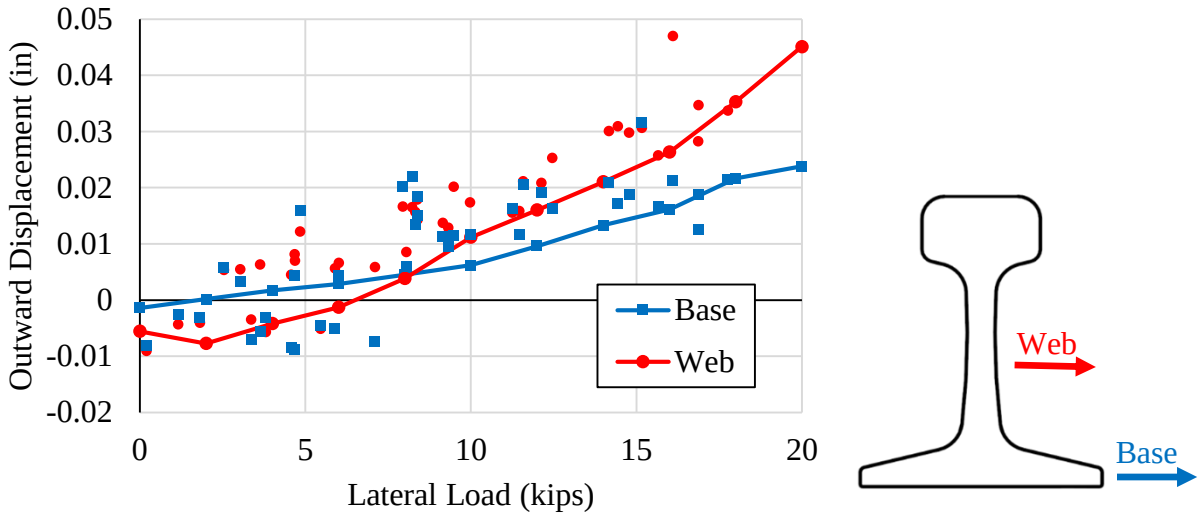

Figure 33: Lateral displacements of the high rail from static and dynamic lateral loads.

Figure 34 shows the compliance of the rail web (i.e. the lateral displacement of the rail base per unit of lateral load) at two rail seats. The plot shows compliance from a freight consist and passenger consist over a curve at multiple speeds.

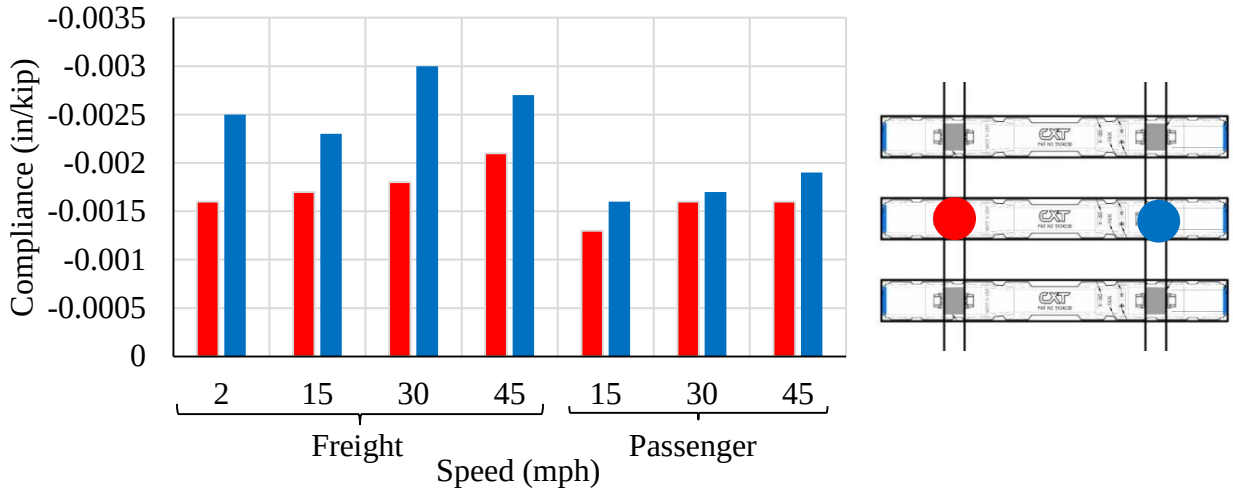

Figure 34: Compliance of rail web laterally to a freight consist on a curve.

Figure 35 shows the compliance of the rail base (i.e. the lateral displacement of the rail base per unit of lateral load) at three rail seats. The plot shows compliance from a freight consist and passenger consist over a curve at multiple speeds.

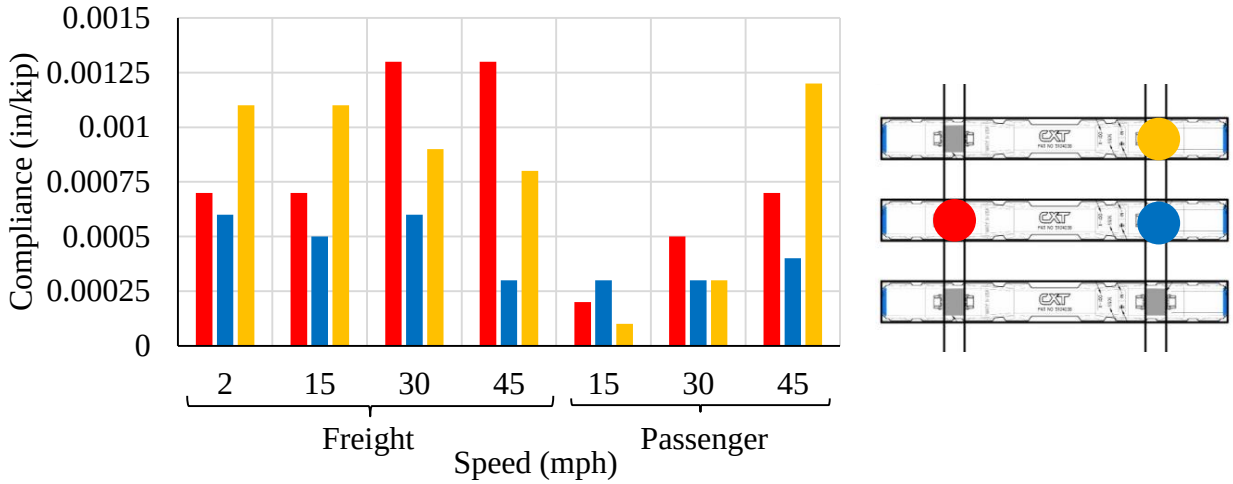

Figure 35: Compliance of rail base laterally to a freight consist on curved track.

3.3 Rail Strains

Figure 36 shows the distribution of vertical web strains centered over adjacent rail seats on the low rail of a curve. This plot shows the response to a 40kip vertical load and 20kip lateral load applied to the center crosstie by the TLV. (Note: positive strains represent tension)

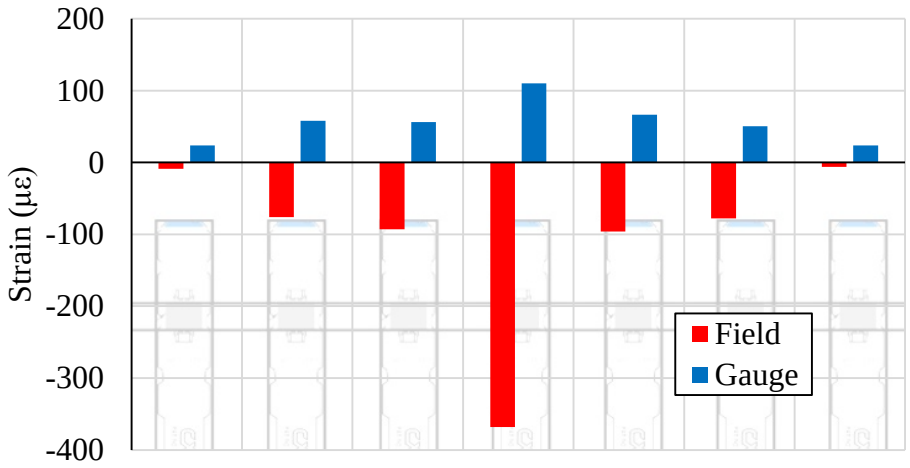

Figure 36: Strains in low rail in adjacent rail seats from 40kips vertical and 20kips lateral load.

Figure 37 shows the distribution of vertical web strains centered over adjacent rail seats on the high rail of a curve. This plot shows the response to a 40kip vertical load and 20kip lateral load applied to the center crosstie by the TLV. (Note: positive strains represent tension)

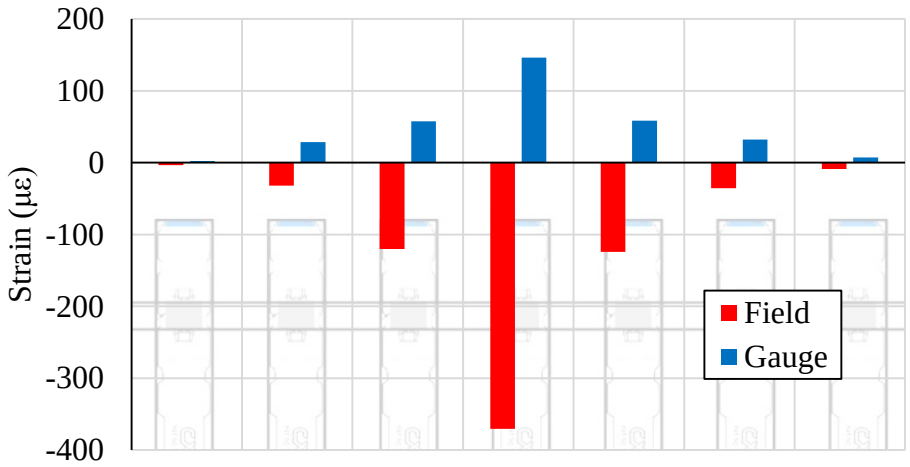

Figure 37: Strains in high rail in adjacent rail seats from 40kips vertical and 20kips lateral load.

Figure 38 shows the distribution of vertical web strains centered over adjacent rail seats on the low rail of a curve. This plot shows the response to a 40kip vertical load applied to the center crosstie by the TLV. (Note: positive strains represent tension)

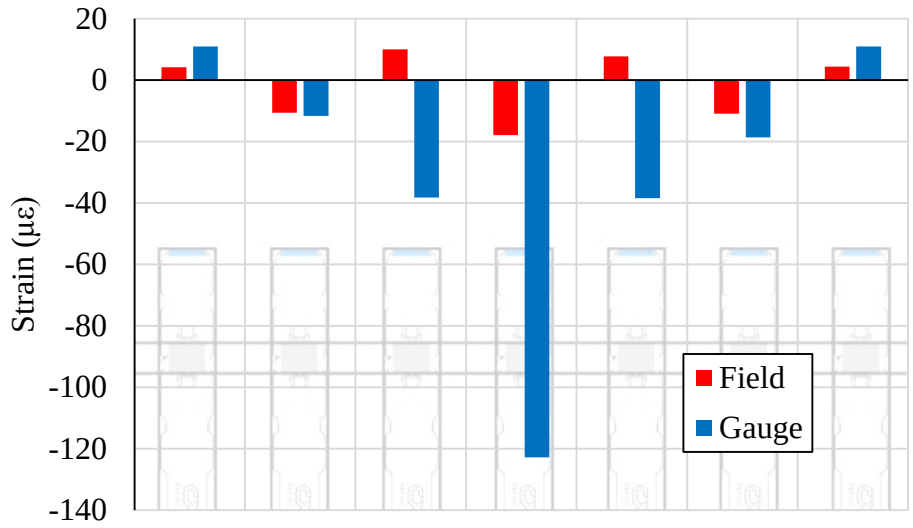

Figure 38: Strains in low rail in adjacent rail seats from 40kips vertical load.

Figure 39 shows the distribution of vertical web strains centered over adjacent rail seats on the high rail of a curve. This plot shows the response to a 40kip vertical load applied to the center crosstie by the TLV. (Note: positive strains represent tension)

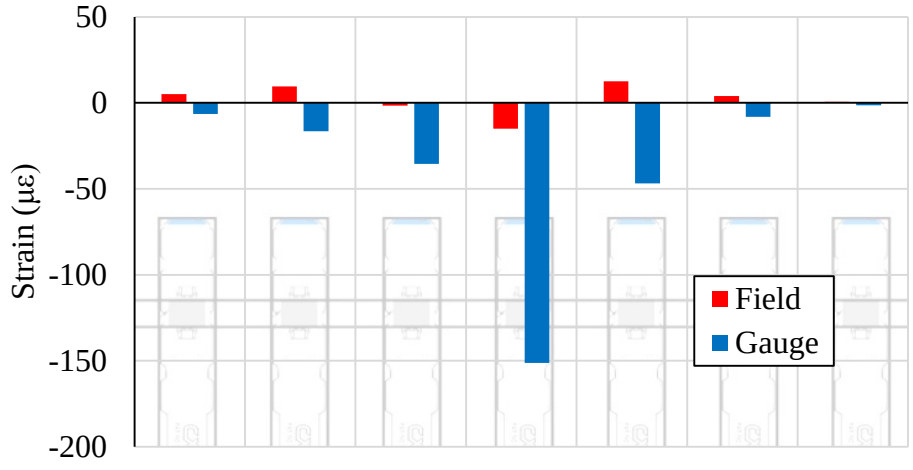

Figure 39: Strains in high rail in adjacent rail seats from 40kips vertical load.

3.4 Fastening Clip Strains

Figure 40 shows clip strains from the each side of a rail seat on the high rail of a curve. Each point is taken from an axle of a freight consist travelling at 45mph. The dotted lines represent linear best-fit lines for each set of data. (Note: positive strains represent tension)

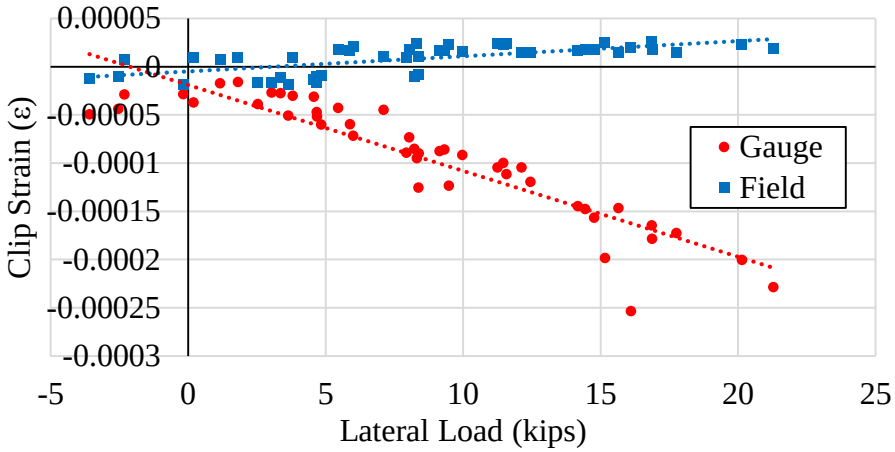

Figure 40: Clip strains on the high rail from lateral loads from a 45mph freight consist.

Figure 41 shows clip strains from the each side of a rail seat on the low rail of a curve. Each point is taken from an axle of a freight consist travelling at 45mph. The dotted lines represent linear best-fit lines for each set of data. (Note: positive strains represent tension)

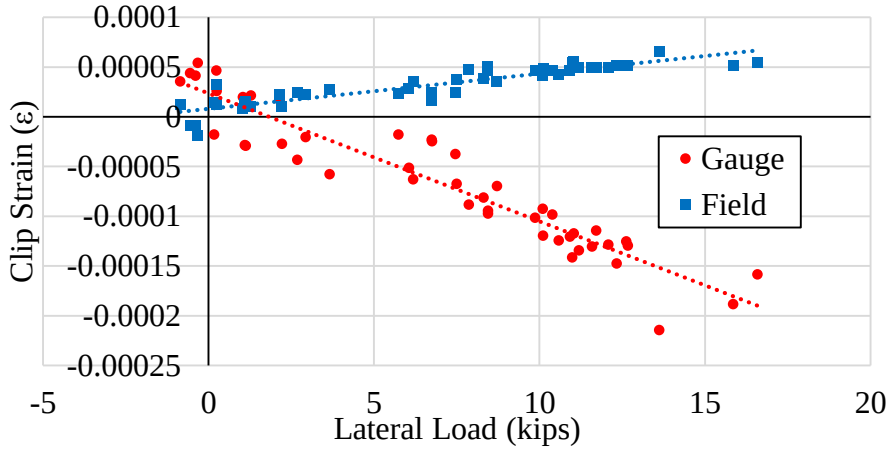

Figure 41: Clip strains on the low rail from lateral loads from a 45mph freight consist.

Figure 42 shows the compliance of the field-side clip (i.e. the strain of the clip per unit of lateral load) at four rail seats. The plot shows compliance from a freight consist over a curve at multiple speeds (2-45mph).

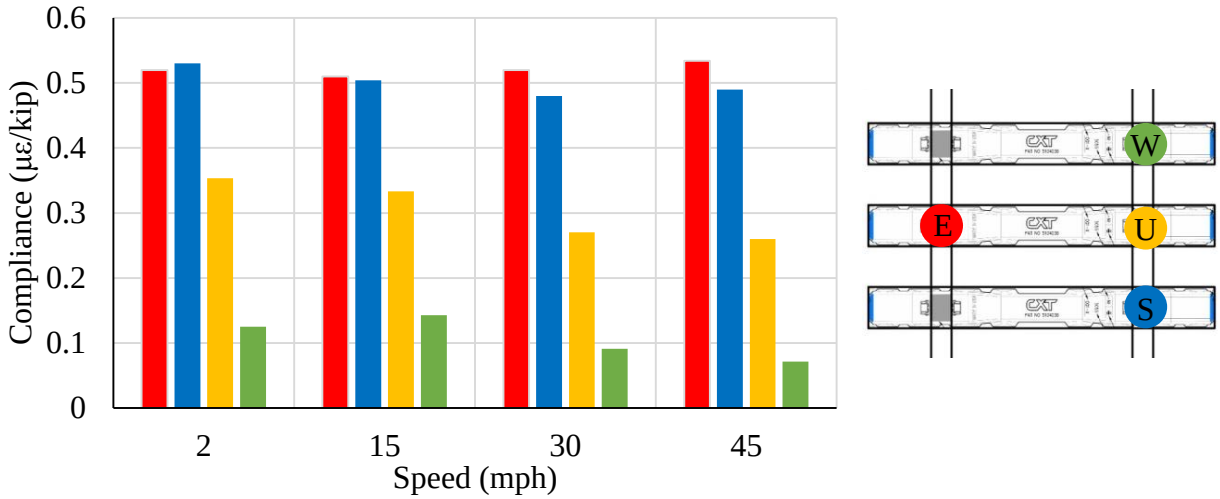

Figure 42: Compliance of field-side clip to a freight consist on a curve.

Figure 43 shows the compliance of the gauge-side clip (i.e. the strain of the clip per unit of lateral load) at four rail seats. The plot shows compliance from a freight consist over a curve at multiple speeds (2-45mph).

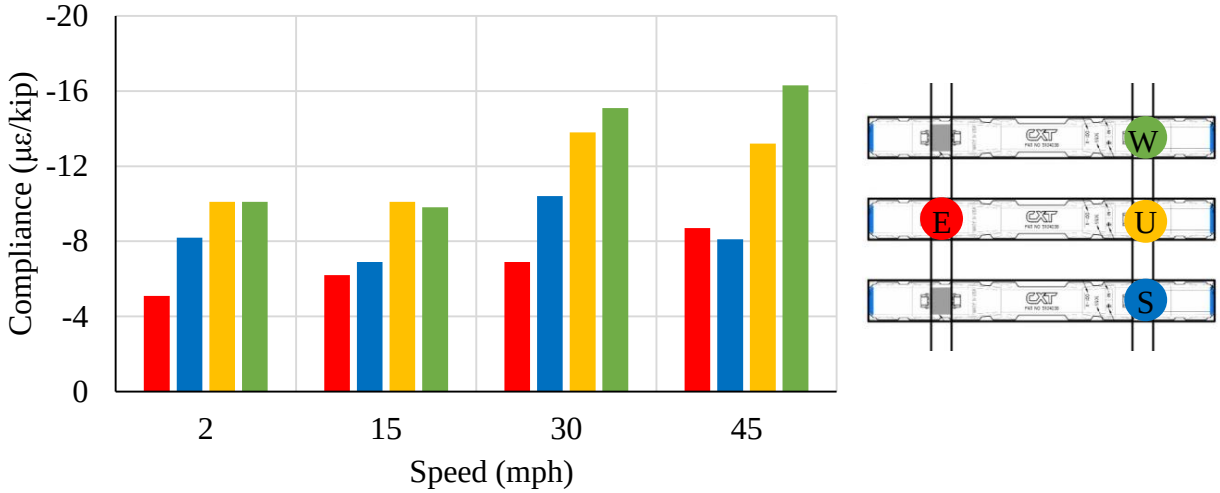

Figure 43: Compliance of gauge-side clip to a freight consist on a curve.

Figure 44 shows the range of clamping forces measured on field and gauge-side clips on curved track from a passing freight consist at 2-45mph. The figure also includes a “typical range” provided by the manufacture, as well as the point at which the clip is expected to yield.

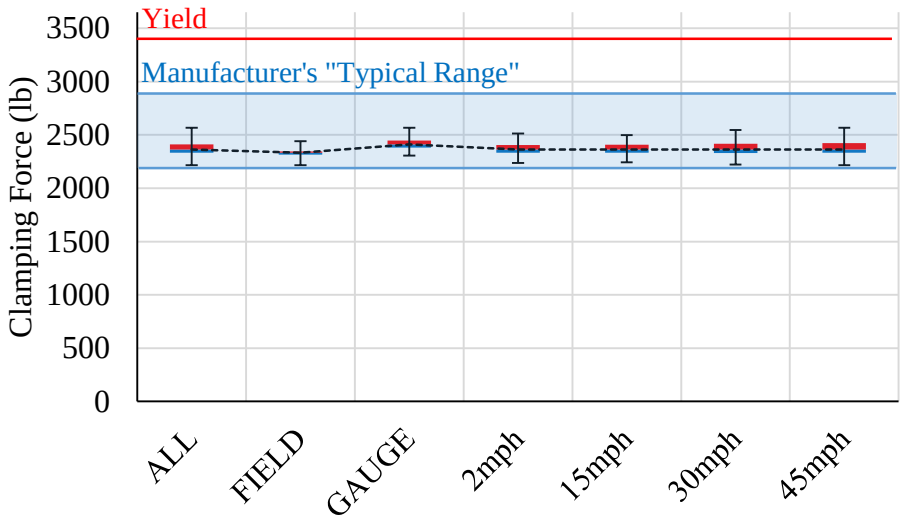

Figure 44: Range of measured clamping forces from a freight consist on a curve.

4. FINDINGS

In order to lay the groundwork for a mechanistic design of the crosstie-fastener system, there must be a general understanding of the load path. In order to detail the analysis in a purposeful matter, this section separates these findings into three separate, interdependent subsets of the system mechanics: the vertical load path, the lateral load path, and component behavior.

4.1 Vertical Load Path

The highest loading demands are vertical gravity loads, especially with heavy freight traffic and impact loads which result from wheel profile imperfections and dynamic truck behavior. Thus there is significant need to understand how this load is being transmitted through the system and shared between adjacent crossties, as well as the many factors as contribute to loading demands (e.g. track modulus, car weight, track curvature).

4.1.1 Vertical Wheel Loads

Vertical wheel loads are the vertical components of the wheel force acting (often eccentrically) on the head of the rail (Figure 45). The static load of a wheel due to car weight is called the nominal wheel load, defined by the American Public Transportation Association (APTA) as "the vertical load on the rail from a wheel when measured on level tangent track". [9] The vertical load of the wheel on the rail often deviates from its nominal wheel load depending on train speed and track curvature (e.g. vertical loads increase on the high rail of curved track as the balancing speed is exceeded). In many extreme cases vertical wheel loads, called impact loads, can far exceed nominal wheel loads primarily due to wheel flats on light cars which allows for very little damping of the track structure. [10] Examples of impact loads from an Amtrak line in

Mansfield, MA are displayed in Figure 46, in which the peak loads can reach as high as 5 times the nominal wheel load.

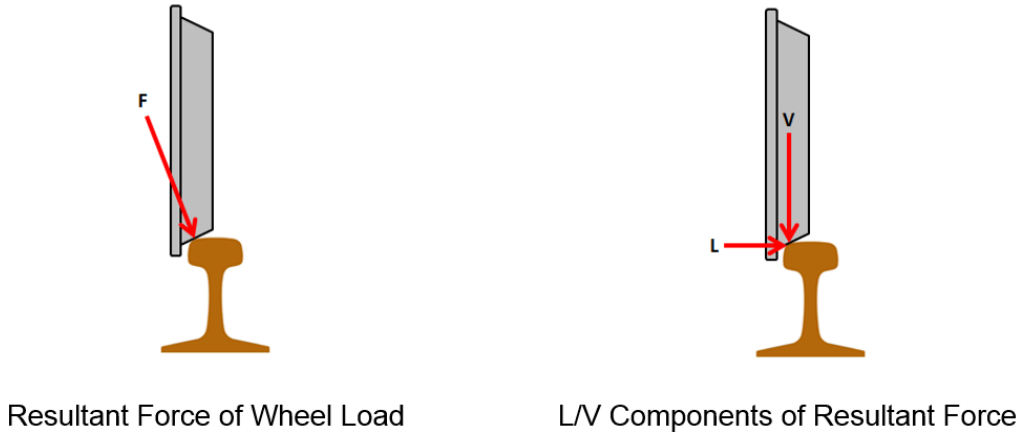

Figure 45: Diagram of wheel load (F) and its vertical (V) and lateral (L) components.

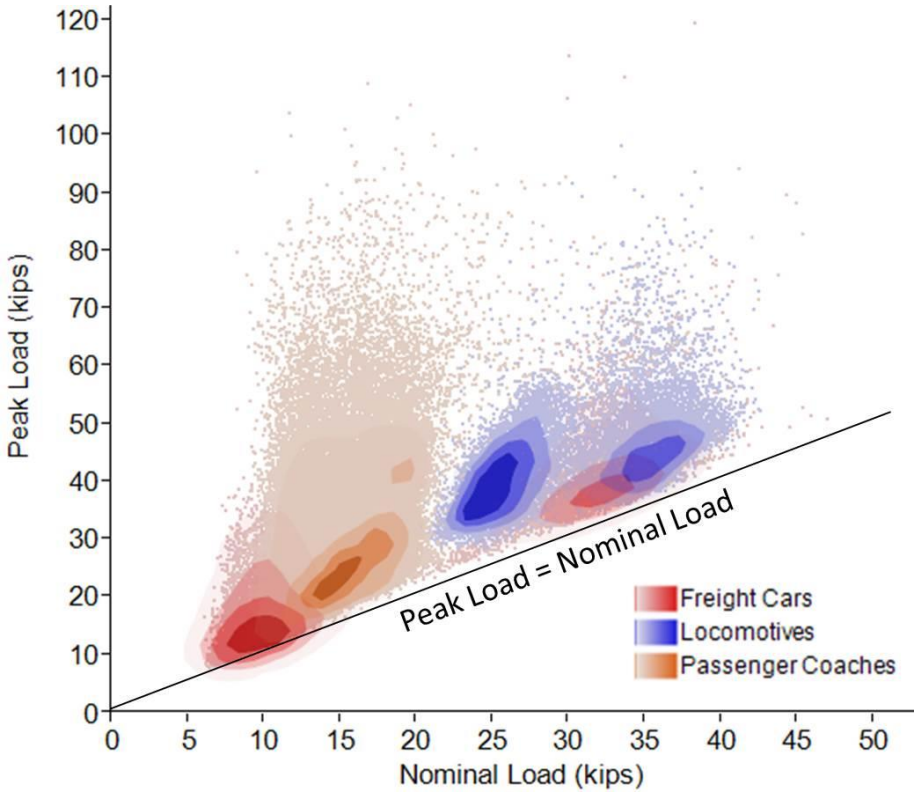

Figure 46: Impact loads and nominal loads measured by a wheel impact load detector (WILD) in Mansfield, MA (courtesy of Brandon Van Dyk and Amtrak, Nov. 2011)

Vertical loads at TTC were measured from a freight consist which consisted of cars weighing 142, 286, and 315kips (nominal wheel loads of 18, 36, and 39kips respectively). Median vertical loads from this freight consist on tangent track were approximately 35kips (Figure 14). With the exception of one load of 60kips, these magnitudes do not exceed 25% of the nominal wheel load. There is also negligible correlation between the average vertical wheel loads on tangent track and train speeds, evident between 15 and 60mph. However, there is an increase in maximum loads (excluding one 60kip impact load at 30mph) from increased vehicle dynamics and vibration.

It should be noted, that this does not address the effects of impact loads, which are largely a product of poorly maintained wheel sets and represent much larger and shorter peak loads. [11] Impact loads are much less common, especially on well-maintained wheelsets provided at TTC and are typically 1.5 times the nominal wheel load, while they are more common in revenue service and are typically on the order of 3-5 times the nominal wheel load. [12] As a result impacts could not be thoroughly investigated in a statistical manner from this specific test program.

The vertical wheel loads measured on curved track are much different and dependent on curve radius. Additional loading demands on the high rail arise from overbalanced speeds due to centrifugal forces acting on the body of the vehicle. Conversely, underbalanced speeds increase the loading demand on the low rail as the superelevation causes the center of gravity to shift nearer to the low rail. Both these extremes are cited as potential contributors to the current failure modes of concrete crossties, specifically rail seat abrasion. [13]

The measured vertical loads imparted by the freight consist on a curved track (with a balancing speed of approximately 33mph) showed the dependency of forces on train speed (Figure 15). At about half the balancing speed (15mph), there was little deviation from the nominal wheel

load. The high rail experienced a modest reduction, and the low rail experienced a slight rise in vertical wheel load. At an overbalanced speed of 45mph, there was a significant increase in the median vertical wheel loads on the high rail (approximately 40% higher than the average nominal wheel loads), which far exceeds the expected loading demands on tangent track. This suggests that there may be a benefit of treating tangent and curved sections of track separately in design. This could include using specialized components or practices to compensate for the increase loading demands (e.g. more robust fasteners or tighter tie spacing). Also at an overbalance speed of 45mph, there was a significant reduction in vertical loads on the low rail (approximately 20% lower than the average nominal wheel load). This poses a different obstacle to design, in that there is an increased lateral to vertical load (L/V) ratio which demands more lateral and rotational restraint, presuming the lateral force remains relatively consistent.

Vertical loads were also measured from a passenger consist, which consisted of cars weighing approximately 87kips (nominal wheel loads of 11kips). Median vertical loads from this passenger consist on tangent track did not deviate much from the nominal wheel loads (11-12kips, Figure 16). However, there were considerably higher impacts measured as high as 2.5 times the nominal wheel load. From observing eighteen train passes on tangent track from 2-102mph, approximately 3% of the vertical loads measured exceeded 1.5 times the nominal wheel load, and 0.5% of the loads exceeded 2.5 times the nominal wheel load.

4.1.2 Vertical Crosstie Displacements

Track deflections are recognized as being a primary indicator of predicting track strength and quality. [14] In the railroad industry, a commonly used measure of substructure stiffness is the modulus of track elasticity, or track modulus. Track modulus is defined as "the load per unit length

of rail required to depress that rail by one unit". [15] Track modulus is also a significant indicator of track stability and contributes to the life of the track system.

Although track modulus represents an all-encompassing value of substructure stiffness, there are more local phenomena that cause variability in the mechanics of the crosstie fastening system, such as inconsistent support conditions from gaps within the ballast structure and localized variability in substructure stiffness. Being that substructure stiffness and crosstie support conditions are such integral parameters in determining rail seat loads, vertical displacements of the crossties were measured. With 40kips of static vertical load applied on a single crosstie, adjacent ties experienced between 50-85% of the center crosstie displacement (Figure 29), suggesting that many more crossties may be engaged.

From displacements of three adjacent crossties, with a 40kip vertical load applied to the end crosstie, different distributions were seen on the low and high rail of the curved track (Figure 30). The low rail showed the highest displacement of 0.14", which far exceeds the optimum displacement (0.05") for quality concrete track. [14] These high displacements are evidence of low substructure stiffness, and potentially a low track modulus. Assuming a linear distribution of the displacements, a range of nine ties were being engaged (showing measurable stresses) at the ballast interface on the low rail. Assuming a direct relationship between displacement and load distribution (i.e. a consistent value of substructure stiffness), the center tie of this section sustained approximately 20% of the load, while the center three crossties sustained a total of 50% of the load at the ballast interface.

The high rail showed indications of stronger substructure stiffness, generating displacements 40% less than the displacements at the low rail. Extrapolating the influence of displacements in a linear distribution, approximately five to seven crossties were being engaged at

the ballast interface. Assuming a direct relationship between displacement and load distribution, the center tie of this section sustained approximately 30% of the load, while the center three crossties sustained a total of 70% of the load.

The dependency of vertical crosstie displacements on train speed was also investigated. Vertical crosstie deflections are plotted against vertical loads measured at various train speeds in Figure 31. The static response from the TLV is also plotted and demonstrates that the range of displacement responses from passing axle loads never exceeded the magnitudes from the static test. This suggests that the static deflection represents a maximum envelope of vertical crosstie deflections with a shorter, more concentrated zone of influence developing below the point of applied load.

4.1.3 Rail Seat Loads

Rail seat loads are the forces distributed to the concrete rail seats below the rail, representing the most significant transfer of vertical load within the fastening system. In practice, this rail seat load as a percentage of wheel load is commonly approximated as 50% for 24" tie spacing. [15] Recent tests conducted by J. M. Sadeghi in 2007 concluded that this transfer load was approximately 57% for a similar spacing. [16] AREMA also provides an estimated percentage of axle load carried by a single rail seat for various tie spacing, shown in Figure 47. This figure estimates the transfer load for 24" tie spacing to be just above 50%. [17]

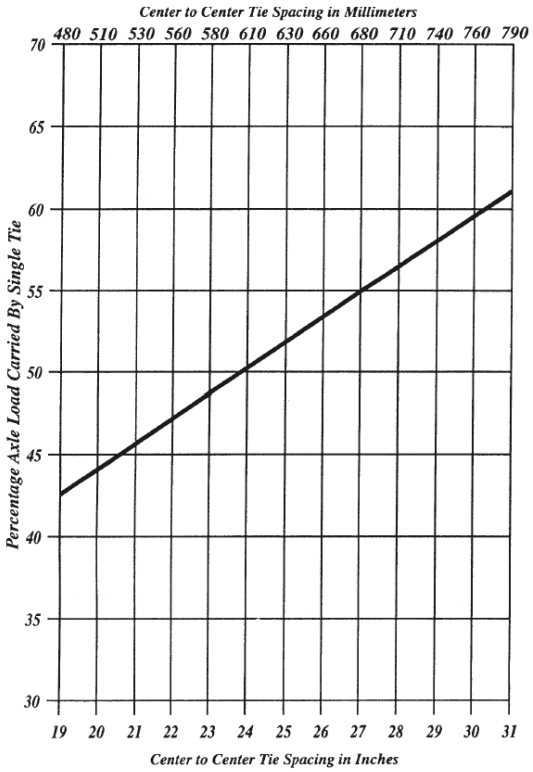

Figure 47: Estimated distribution of loads (AREMA 2012).

From the freight consist with an average nominal wheel load of 36kips, median rail seat loads measured at one rail seat on tangent track ranged from 16-20kips, or about 50% of the nominal wheel load (Figure 17), which agrees with the estimated transfer load in standard practice. With increasing train speed (from 15 to 60mph), there was an increase of 4kips of rail seat load, representing an increase of 10% of the nominal load. Rail seat loads at higher speeds also show an increase in variability; the range of the center 50% of measured rail seat loads increases from 3kips to nearly 10kips. The increase of the magnitude and variability of the rail seat loads can be explained by the numerous dynamic effects which are a result of numerous factors: roll, slip, wheel irregularities, shock, unequal distribution of lading, and vibration. [15]

From the analysis of four adjacent locations, the rail seat load as a percentage of the wheel load shows significant variability, which correlates with track stiffness (Figure 26). The average

rail seat load transfer measured from the freight consist over tangent track varied from 15 to 50%. The three adjacent rail seats had similar load transfers (about 40-50%) and the ends of the crossties at those locations showed deflections of approximately 0.06". The rail seat on the opposite end of the center crosstie had a considerably lower transfer of load (about 13%) and a vertical deflection of 0.12", evidence of a low substructure stiffness. With this reduced track stiffness and a potential gap between the end of the crosstie and top of the ballast, there is increased flexure in the rail from a more compliant substructure. This allows for more of the vertical load to be transferred to adjacent rail seats as well as the strain energy associated with bending of the rail.

To further illustrate their dependency on support conditions, rail seat loads were plotted against vertical crosstie displacements from static tests conducted using the TLV, as shown in Figure 27. From this testing, the high rail shows characteristics of a high track modulus, while the low rail shows characteristics of a low track modulus. The rail seat on the high rail with the stiffer substructure shows low vertical crosstie displacements, which results in higher rail seat loads. Conversely, the rail seats on the low rail with high vertical displacements showed very low rail seat loads. From these weakly supported sections, the rail is allowed to displace significantly before the rail seat is fully engaged, generating higher rail seat forces with increasing displacements. This initial and dramatic increase in displacement represents the overcoming of a gap in which the crosstie is not fully engaged until it displaces enough to eliminate this slack in the system.

The rail seat loads of the freight train measured on the curved track shows much lower rail seat load transfers on average (Figure 28). The rail seat load transfer on the high rail was approximately 30%, while the load transfer on the low rail was approximately 20%. Even with increasing train speeds, these transfer loads remained consistent. The measured vertical crosstie

displacements on the curved track were also 40% higher on average than the vertical displacements on the tangent track.

Rail seat loads were also measured from the passenger consist with an average nominal wheel loads of 11kips on tangent track (Figure 18). At lower speeds (15-50mph), median rail seat loads were between 4-5kips (45% of the nominal wheel load). This is agreeable with the estimated 50% load transfer in most literature. Median rail seat loads decreased at higher speeds (80-102mph) to about 30% load transfer. The range of rail seat loads also increased with increasing speed, as a result of the numerous aforementioned dynamic effects of the car body.

Some of the observed variability at higher speeds (over 45mph) is inconsistent with the measurements from the embedment gages within the crosstie (2.3.6) and MBTSS (2.3.11). When measuring rail seat loads from shear strains of the rail there are several outliers which can disagree with these two other methodologies for measuring relative rail seat forces. It should be noted that the methodology for calculating rail seat loads assumes that the vertical wheel load acting over the rail seat is identical to the wheel load recorded in the adjacent crib (as discussed in 2.3.2). Thus an excessive load realized in one section and not the other leads to an erroneous measurement of rail seat load, and as shown in the loading data, the higher the train speed the more likely the chance for dynamic variability of these loads.

4.1.4 Vertical Load Distribution

Thus far vertical load distribution has been explored using two approaches: vertical crosstie displacements and rail seat loads. Using the low rail of the curved track as an example, the center crosstie makes up 20% of the stresses at the crosstie-ballast interface and 25% of the forces at the rail seat. This magnitude of load percentages suggests that about seven to nine

crossties are being engaged. There is also a damping of the load as the vertical load is being transferred into crossties and down into the ballast.

Vertical load distribution has also been investigated at the rail level, using the vertical web strains outlined in section 2.3.10. The relative distribution of rail stresses shows that the load is more distributed in the low rail (Figure 36) than in the high rail of a curve (Figure 37) in response to a static load of 40kips vertical and 20kips lateral. These distributions are also shown for the case with just a 40kip vertical load (Figure 38 and Figure 39). Although each load seems to be transferred over about five crossties in each case, more strain is seen at the outside crossties for the low rail, which shows a wider distribution of crosstie displacements as was seen in the distribution of vertical crosstie displacements.

Assuming that the average strain from each side of the rail represents a relative quantity of vertical load, there is approximately 66% of load being transferred to the center tie on the low rail from the 40kip vertical load and 63% from the 40kip load with the additional 20kip lateral load. These percentages are much greater than the 20% and 25% transfer loads determined by the vertical crosstie displacements and rail seat load methodology, respectively. This distribution of rail stresses provides a look of the vertical compressive forces travelling through the rail web, prior to entering the fastening system.

4.2 Lateral Load Path

Although their magnitudes represent a fraction of the vertical loading demands, lateral loads are the most demanding on the fastening system. In particular, lateral loads apply large bending moments to the rail, which requires rotational restraint which is provided by the fastening system. [5] In recent years, the lateral load path through the crosstie-fastener system has gained considerable interest in order to mitigate problems such as rail seat abrasion, shoulder wear,

insulator post failure, etc. These lateral demands are influenced mainly by curve radius, train speed, wheel-rail interface, and suspension characteristics of the trucks. [*18*]

4.2.1 Lateral Wheel Loads

On tangent track, there are two significant lateral loads that have been observed. First from most axles there is a modest outward lateral load applied to the rail. From the freight consist these loads are approximately 2.5kips as shown in Figure 19. In addition, there are often negative (applied inward towards the gauge) or negligible loads observed, representing about 20% of the total lateral loads measured from twelve train passes from train speeds of 2 to 45mph. While over 75% of the outward lateral loads from freight are below 3.5kips, one of about forty axles will impart about a 6kip lateral load. However, on tangent track, there is negligible correlation between these lateral wheel loads and train speed between 15 and 60mph. This suggests that train speed should not be a heavily weighted factor in the design of tangent track.

Median lateral loads on curved track from the same freight consist are significantly greater (2-5 times as large on average, as shown in Figure 20 and Figure 21). Additionally, lateral loads on curved track are heavily dependent on train speed. Lateral loads nearly double on the high rail as the balancing speed (about 33mph) is exceeded. On the low rail, there is a slight reduction in median lateral loads, while maximum loads remain relatively unchanged. The differences in magnitude and behavior of lateral demands on each track type suggest that there should be significantly higher lateral loading demands on curved track than on tangent track in design.

In order to design fastening systems to resist lateral loading demands, it is worth developing a way to predict the magnitude of lateral load (from the design vertical loads, for example). In order to observe the dependency of lateral loads on vertical loads, each load was plotted for each axle of a freight consist travelling at various speeds on tangent and curved track.

On tangent track (Figure 22), there appears to be no strong correlation between concurrently acting vertical and lateral wheel loads. On curved track, however, there is an evident relationship. On the high rail (Figure 23), there is a positive correlation between lateral and vertical wheel loads. The low rail (Figure 24), shows a slight negative correlation between lateral and vertical wheel loads. The figure also shows the increase of vertical loads on the high rail and reduction of vertical loads on the low rail with increasing train speed as described in section 4.1.1.

The trendlines showing correlation between lateral and vertical wheel loads on both the high and low rail are shown together in Figure 25. These lines represent the range of concurrent lateral and vertical loads you would expect from similarly weight railcars. Note that around the balancing speed (30mph), the vertical loads on the high and low with no lateral load converge to 35kips (about the 36kip average nominal wheel load). This plot also demonstrates a concern for the loading demands on low rail, and that is as the lateral loads increase there is less concurrently acting vertical load (especially at higher train speeds). This translates to a higher lateral to vertical load (L/V) ratio, which is more demanding on the fastening system as more bending forces are being applied to the rail with less normal force to "pin" the rail to the crosstie. This puts an increased amount of the lateral and rotational demand on the fastening system, in particular to the field-side shoulder and gauge-side fastening clip.

4.2.2 Lateral Load Distribution

From the July 2012 test, no direct measurements were taken of lateral load transfer. However, just as the vertical web strains were used in determining vertical load distribution, lateral load distributions can be interpreted in a more qualitative fashion. When lateral loads are applied to the rail, the tensile bending stresses of the rail web on the gauge-side surface exceeds the compressive stresses due to an eccentric vertical force. These bending stresses also cause

increased compressive stresses on the field-side surface, providing strain values which can be used to interpret the extent of rail bending due to lateral loading (as shown qualitatively in Figure 48).

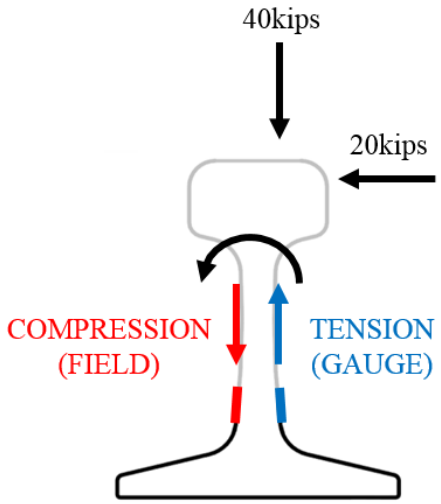

Figure 48: Rail web stresses from vertical and lateral loading.

Comparing the distributions of gauge-side tensile stresses in the web of the rail, for the high rail under a static 20kip lateral force, there is a distribution of five crossties (Figure 37). With the same load on the low rail, there is a flatter and wider distribution across seven crossties (Figure 36). As noted earlier, the high rail has a considerably stiffer substructure. This stiff substructure results in higher rail seat forces and a "pinning" of the rail to the crosstie. This "pinning" provides restraint from rotation, thus limiting the ability of the system to distribute lateral loads to adjacent crossties and causing more bending stress within the rail. Essentially, the rail seats which have lower rail seat loads behave as if they are resisting lower "effective" L/V ratios, although the input L/V ratio is the same in each case.

4.2.3 Lateral Rail Displacements

Lateral rail displacements were measured to understand the lateral resistance of the crosstie-fastening system to lateral loading for a particular design. Both the static and dynamic

measurements resulted in similar displacement responses (Figure 32 and Figure 33). In particular the stiffness of the rail (amount of lateral load required to displace the rail a unit distance) is almost the same as recorded from the static TLV tests and from train passes. The only significant difference between the static and dynamic displacements is that the web displacements measured in the low rail showed a higher range of values. However, this can be attributed to the displacement of the rail due to an eccentric vertical load induced by the TLV, which causes inward deflections. If a similar eccentricity is not matched by a passing axle, this creates an offset. For example, in Figure 32, there is 0.1" inward displacement from the eccentric 40kip vertical load, before applying any lateral force. Thus if the contact patches of the passing wheels were closer to the center of the rail (reducing eccentricity) or the magnitudes of vertical loads were not as high as 40kips (which most nominal axle loads were not), you would expect higher outward displacements.

Figure and Figure also show the linearity of the lateral loads to rail displacements. This high correlation suggests that the system behaves linearly to input loads, easing the mechanistic and computational analysis of the system as well as providing the potential for evaluative testing in commercial use. The slopes of these curves represent compliance (the inverse of the stiffness of the rail to lateral displacement). When comparing these compliances at various locations and train speeds, the web displacements seem to be generally uniform and unique to each rail seat (Figure 34). This is a good indicator that there exists a consistent lateral stiffness per rail seat, which can be used in performing parametric analyses (e.g. comparing fastening systems and rail pads).

The compliance of the rail base is much more sensitive to train speed and shows significant variability within the same rail seat (Figure 35). On average these base displacements are 25% the

magnitude of web displacements, and even lower with the lighter passenger axles. Thus the signals approach the resolution of the sensors and susceptibility of other minor influences to noise.

With a third point of reference (e.g. vertical displacement of the rail base), the real-time motion of the rail can be captured. This would provide an understanding of how the rail is rotating and translating as a rigid body. Because the vertical displacements were not accurately captured in the July 2012 testing program, this analysis has not yet been started.

4.3 Component Behavior

Many of the failures in concrete crossties are specific to component failure. When a component fails (e.g. a deteriorated pad or insulator), there is more movement allotted in the system. This increased movement can lead to degradation mechanism such as rail seat deterioration, abrasion of the insulator or iron shoulder, and yielding of the fastening clip. [19] There is also a need to look at specific components in isolation, such as the crossties, which have many characteristics that are mostly independent of the fastening system (e.g. resistance to bending moments). This section details measurements of the fastening clips and crossties.

4.3.1 Fastening Clip Behavior

The fastening clip, often referred to as a "spring clip", is essential for affixing the crossties to the rail and controlling translational and rotational movement of the rail. [19] The fastening clip primarily behaves as a cantilever, in which two "clip toes" bear against the surface of the insulator (Figure 49). Utilizing a simplified approach of one strain measurement, clamping force was determined. In order to relate this isolated surface strain with a clamping force, the UIUC computational model was utilized. [20] From the finite element model of the fastening clip, a linear relationship (approximately 0.839 lbs/με) was made between this particular strain on the clip and

the associated clamping force with a coefficient of determination of 0.9999, which was used in determining changes in the clamping force (Figure 50).

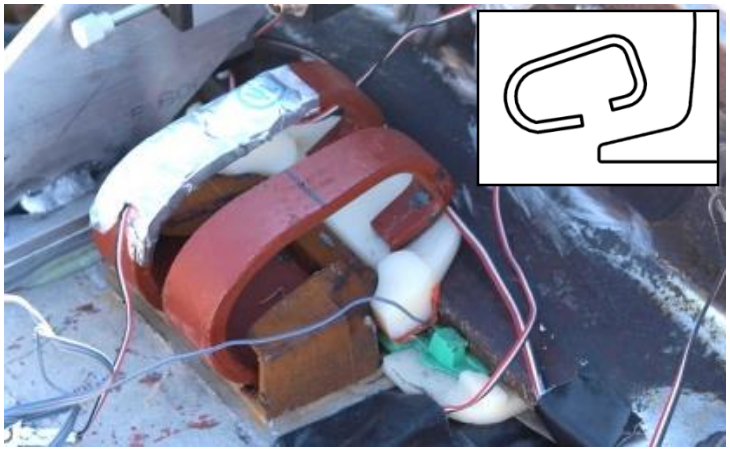

Figure 49: The elastic fastening clip (in service with instrumentation).

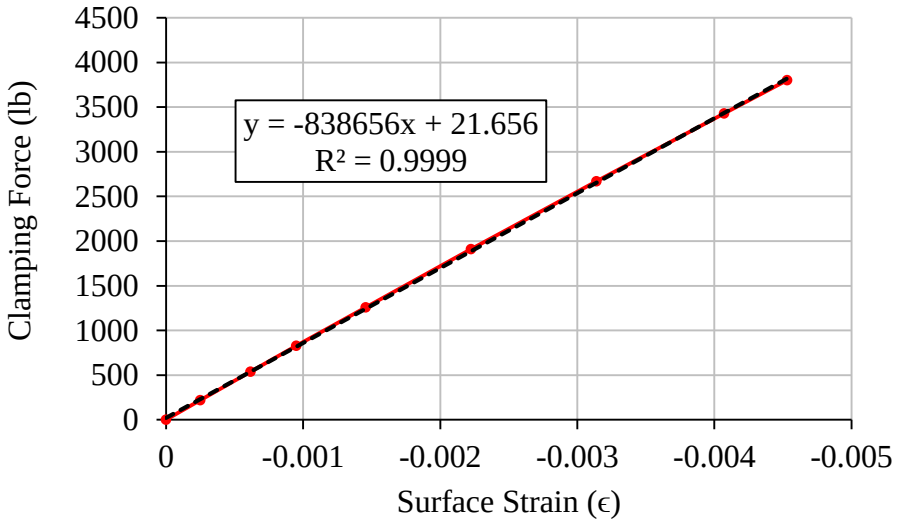

Figure 50: Correlation between clamping force and clip strain.

When lateral load is applied to the rail, gauge-side clips show an increase in clamping force, while field-side clips show a reduction in clamping force. This occurs because the lateral load causes the rail to rotate about its longitudinal axis. The only resistance to the resultant uplift of the gauge-side rail base is the gauge-side clip, which then applies a greater clamping force.

Meanwhile the field-side rail base is applying downward pressure onto the rail pad as the rail rotates. This causes vertical displacement of the rail pad, which allows for a reduction of the demand on the field-side clip lowering the clamping force. With low L/V ratios (less than 0.05), a relaxation of each clip is measured as pad compression dominated the behavior from a mostly vertical load.

It is desirable for the mechanistic design process, as well as for computational analyses, to simplify the fastening clip and treat it as a linear elastic spring. To do determine the accuracy of that assumption, measured clip strains were plotted against measured lateral wheel loads (Figure 40 and Figure 41). The coefficient of determination for these plots was 0.86, on average. This high correlation suggests that the fastening clips behave similar to linear elastic springs. This assumption serves to simplify the mechanistic behavior of the clip when following the load path, and reinforces the understanding that the primary function of the fastening clip (aside from maintaining longitudinal stability) is to resist lateral forces. Also, in order to simplify the computational effort of a comprehensive finite element, this finding serves to reinforce the assumption that clips can be treated as elastic springs in place of an elaborate finite element model, especially in multi-crosstie applications.

The slope of the lateral load-clip strain plots also provides a measurement of compliance (i.e. strain/load). These compliances are shown in Figure 42 and Figure 43 for field-side and gauge-side clips, respectively. The compliance of each clip do not show a strong dependency on speed, and are relatively similar for each clip. However, there is an apparent difference in compliances of clips on Rail Seat W (green) and a lesser distinction on Rail Seat U (yellow). The field-side clip is significantly lower than the others (about 20% of other compliances), and the gauge-side clip compliances is the highest. This is the only rail seat in the test section which had

an MBTSS sensor in the rail-pad interface, which is comprised of a low-friction, Teflon layer. It has been shown in laboratory tests at UIUC that the use of this Teflon surface vastly increases the lateral loads imparted to the insulator, as no load is being resisted by pad friction.

The range of clamping forces as recorded by the clip strains is shown in Figure 44. These clamping forces are measured in the most extreme loading environment of the testing: a heavy freight train on curved track. These measurements showed that the fastening clips were conservatively designed, relative to the "typical range" of clamping forces provided by the manufacturer, and well below yielding (the point at which the clip experiences enough plastic deformation that it cannot restrain the rail). The figure also demonstrates that gauge-side clips, which make up 75% of fastening clip failures in service, have significantly higher demand. Other factors that may cause further demand on the fasteners include high track curvature, low modulus rail pads, which allow for more rail movement. [21]

4.3.2 Crosstie Bending Moments

As mentioned in section 2.3.7, there is ongoing analysis of crosstie surface strains in order to understand bending moments of the crossties below the rail seat areas and at the tie centers. These measurements are integral in improving the design procedures for AREMA regarding design moments. In the standard European code (EN 13230) design moments at the rail seat are 31% lower than those in accordance with AREMA. [22] In addition, the design moments at the tie center stipulated by AREMA is 17% lower than the European code. [23] This suggests a significant opportunity for an understanding in moment distributions, both in terms of probabilistic conditions and an understanding of the factors that contribute to high bending moments.

A significant barrier to calculating bending moments using the surface strain gages has been determining the elastic modulus of concrete, particularly in the context of a prestressed

section. Elastic moduli of the concrete from center-positive and center-negative bending tests in the lab at UIUC have shown moduli over 9000ksi, much greater than the predicted modulus of 6000ksi. Efforts are being made to further understand this modulus and better predict bending moments.

Meanwhile, the lab tests for center-positive and center-negative bending have been used as a calibration to calculate moments seen in the field. Some crossties showed different moment distributions in response to the same load. For example, Figure 51 demonstrates positive and negative moment being measured at the left rail seat due to the same axle acting at 60mph. There was also a general increase in moments as speed increased. This is true for the crosstie in Figure 52, which shows the moment distributions from the same axle on a passenger train travelling from 15 to 102mph. Lastly the variability in the type of moment distribution from tie to tie was severe. As you can see comparing Figure 51 and Figure 52. This is a product of widely variable support conditions on newly installed track, which is evidence in the wide range of crosstie deflections mentioned earlier in section 4.1.2. [*24*]

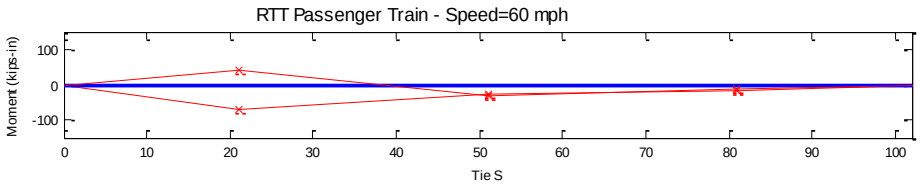

Figure 51: Bending moment distributions along a concrete crosstie from the same axle load.

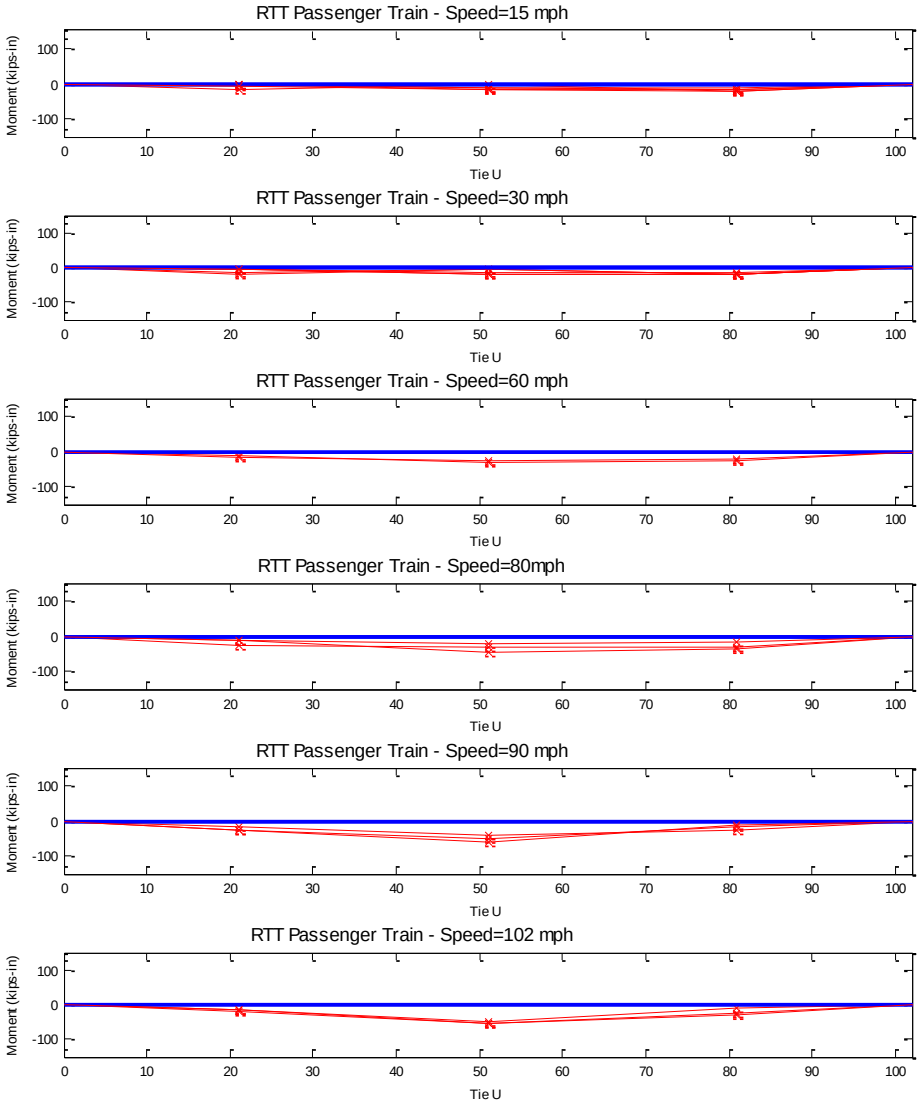

Figure 52: Bending moments along a concrete crosstie at various speeds.

5. CONCLUSION

Vertical loading demands on tangent track showed negligible deviation from nominal wheel loads. Measured impact loads were higher from the lighter-weight passenger consist as a percentage of nominal wheel loads than the freight consist (150% to 125%) and occurred more frequently as a percentage of total axles (6% to 3%). Neglecting the effects of impact loads, there was no correlation between vertical loads and train speed on tangent track.

Vertical loading demands on curved track were significantly higher than on tangent track. At an overbalanced speed of 45mph, vertical wheel loads on the high rail exceeded the nominal wheel load by 40% from the centrifugal forces acting on the body of the railcar to shift the weight nearer to the high rail. At the same speed, loads on the low rail were reduce by 20% of the nominal wheel load, which represents a higher L/V ratio as lateral forces remained relatively consistent.

Vertical crosstie displacements suggested high variability of stiffness within the curved section, with high rail displacements 40% lower than low rail displacements for the same input loads. From vertical tie deflections compressive stresses at the crosstie-ballast interface were approximated to span a wide range of seven to nine crossties. Assuming uniform stiffness across the same ends of adjacent crossties, crosstie-ballast stresses at the center crossties account for 20 to 30% of the load, and the center three crossties account for 50 to 70%. These static deflections also represented the maximum magnitude of deflections when compared with dynamic tie displacements.

Typical rail seat forces measured from a freight consist on tangent track ranged from 44-56% of the vertical wheel load. However, with low substructure stiffness and/or slack below a particular rail seat, transfer forces were generated as low as 15%. In all cases, higher

substructure stiffness (low crosstie deflections) resulted in higher rail seat loads. In the most extreme case of static loads as high as 95% of the wheel load was transferred to the rail seat on the high rail of a curved track. On the low rail 25% of the load was transferred to the rail seat with the same loading conditions and tie deflections measured 40% higher. The variability of rail seat forces also increased with increasing speed, as vertical loads are more susceptible to increases from vehicle dynamics.

Vertical web strains suggest a slightly smaller zone of influence than the crosstie displacements (about five crossties). The vertical compressive stresses in the web above the center crosstie represents about 65% of the total load transferred within the rail web. This represents the undamped flow of forces above the rail base.

Lateral loading demands are significantly higher on curved track than tangent track, with median lateral loads two to five times as high as those on tangent track. Lateral loads also show a significant dependence on train speed for curved track, but negligible dependency on train speed for tangent track. On the high rail, as train speeds exceed balancing speed the lateral loads double in size from the lower speed magnitudes, which are already twice as high as lateral loads measured on tangent track. On the low, lateral loads are 2.5 times as high as those on tangent track and decrease slightly with increasing train speed.

Using vertical web strains, lateral loading demand was detected by the magnitude of gauge-side tension. The spread of lateral loads was similar to the vertical distribution of five crossties. Higher substructure stiffness caused he spread of rail bending due to lateral loads to be reduced, concentrating the bending at the center crosstie. This may be a product of higher “pinning” forces on the rail, which cause for a lower effective L/V ratio.

The lateral displacements of the rail base and web showed a good correlation with lateral wheel loads. This suggests a lateral stiffness exists unique to the rail seat, which can be used in parametric studies to compare factors that influence resistance to rail translation and rotation. Also, measured web displacements were 4 times larger than base displacements, suggesting significant rigid body rotation of the rail.

Using a single strain gage on the top surface of the fastening clip, clamping forces were measured. The responses of the fastening clip were highly linear with lateral loads as well, verifying the assumption that the clip behaves as an elastic spring. Also, under the most extreme testing conditions (heavy freight consist on curved track), the clamping forces generated were on the low end of the "typical range", suggesting a conservative design.

REFERENCES

[1] International Heavy Haul Association. Guidelines to Best Practices for Heavy Haul Railway Operations, Infrastructure Construction and Maintenance Issues. D. & F. Scott Publishing, Inc. North Richland Hills, Texas, 2009.

[2] FIB, 2006, Precast concrete railway track systems. International Federation for Structural Concrete (fib). Sprint-Digital-Druck. Stuttgart, Germany.

[3] Zeman, J.C., Hydraulic Mechanisms of Concrete Tie Rail Seat Deterioration, M.S., University of Illinois at Urbana-Champaign, Urbana, Illinois, 2010.

[4] Van Dyk et al 2012, International Concrete Crosstie and Fastening System Survey – Final Results, University of Illinois at Urbana-Champaign, Results Released June 2012

[5] Hanna, Amir, 1975, Railway Track Research – Theoretical and Experimental. Portland Cement Association 1975. Skokie, IL.

[6] Van Dyk, B. J., et al., 2009, Considerations for the Mechanistic Design of Concrete Sleepers and Elastic Fastening Systems in North America. Paper presented at the Proceedings of the International Heavy Haul Association Conference, IHHA 2013.

[7] ARA, Inc., ERES Consultants Division, Guide for Mechanistic-Empirical Design of New and Rehabilitated Pavement Structures, Champaign, Illinois 2004.

[8] Ahlbeck, D., M. Johnson, H. Harrison, & R. Prause, 1976. Pilot Study for the Characterization and Reduction of Wheel/Rail Loads. U.S. Department of Transportation, Springfield, VA.

[9] APTA Commuter Rail Executive Committee, 14. APTA SS-M-014-06: Standard for Wheel Load Equalization of Passenger Railroad Rolling Stock, The American Public Transportation Association, Washington, D.C. 2007.

[10] Prause, R. H., & Kish, A., 1978, Statistical Description of Service Loads for Concrete Cross Tie Track, 57th Annual Meeting of the Transportation Research Board, January 1978.

[11] Moody, Howard G., 1987, Dynamic Wheel Load Detector Extends Life of Railroad Ties. TR News, (January-February 1987), pp. 8-9.

[12] Harrison, H. D., et al., 1984, Correlation of Concrete Tie Track Performance in Revenue Service and at the Facility for Accelerated Service Testing, FRA/ORD-84/02.1, Federal Railroad Administration, Washington, D.C., August 1984

[13] Reiff, R., 2009a, "Evaluation of Concrete Tie Rail Seat Abrasion Detection/Measurement Systems," AAR Research Report RS-09-001.

[14] Anderson, J. S., & Rose, J. G., 2008, In-situ test measurement techniques within railway track structures. Paper presented at the Proceedings of the ASME/IEEE/ASCE Joint Rail Conference, JRC 2008, 187-207.

[15] Hay, W.W., 1982. Railroad Engineering, 2nd ed., John Wiley & Sons, Inc., New York City, New York, Ch. 23, pg. 253 and 448.

[16] Sadeghi, J., 2008, Experimental evaluation of accuracy of current practices in analysis and design of railway track sleepers. Canadian Journal of Civil Engineering, 35 (9), pp. 881-893

[17] AREMA Manual for Railway Engineering, 2009, American Railway Engineering and Maintenance-of-Way Association (AREMA), Landover, Maryland, v 1, Ch. 30.

[18] Handbook of Railway Vehicle Dynamics, 2006, CRC Press, Taylor & Francis Group, Boca Raton, Florida, pp. 212.

[19] Lutch, R., 2009, Capacity Optimization of a Prestressed Concrete Railroad Tie, M.S., Michigan Technological University.

[20] Chen, Z., Shin, M., & Andrawes, B., 2013, Finite Element Modelling of the Fastening Systems and the Concrete Sleepers in North America, presentation at the 10th International Heavy Haul Association Conference, New Delhi, India, February 2013.

[21] Hadden, J. D., Prause, R. H., & Harrison, H. D., 1979, Field Tests for the Failure Evaluation of PANDROL Rail Fasteners, U.S. Department of Transportation, Cambridge, MA, August 1979.

[22] EN 13230. Railway applications - Track - Concrete sleepers and bearers. Edition 2002. European Committee for Standardisation.

[23] Freudenstein, S., 2007, Concrete Ties Designed for High Dynamic Loads, Presented to the American Railway Engineering and Maintenance-of-Way Association (AREMA), Neumarkt, Germany, 2007.

[24] GeMeiner,B., & Mattson, S., 2005, Wheel Impact Loads and Transmission into Track Structure, Presented at Transportation Research Board 2005 Annual Conference, January 2005.

APPENDIX A: EQUIPMENT

Table A1: List of equipment (data acquisition and sensors).

Equipment	Function	Manufacturer
Compact DAQ	Data Acquisition	National Instruments
NI 9235*	Quarter bridge strain gage module	National Instruments
NI 9237*	Full bridge strain gage module	National Instruments
NI 9205*	Voltage module (potentiometers)	National Instruments
Weldable strain gages (axial)	Vertical web/ transverse strains	Hitec Products, Inc.
Weldable strain gages (axial)	Vertical/lateral load circuits	Hitec Products, Inc.
Strain gages (linear, 120Ω)	Clip strains	Micro-Measurements
Concrete strain gages	Crosstie surface strains	Micro-Measurements
Embedment strain gages	Internal rail seat strains	Micro-Measurements
Linear potentiometers (TRS-25)	ALL displacements	Novotechnik

*Compact DAQ analog input modules

Figure A1: National Instruments Compact DAQ.

Figure A2: Compact DAQ analog input modules: NI-9237, NI-9235, and NI-9205 (left to right)

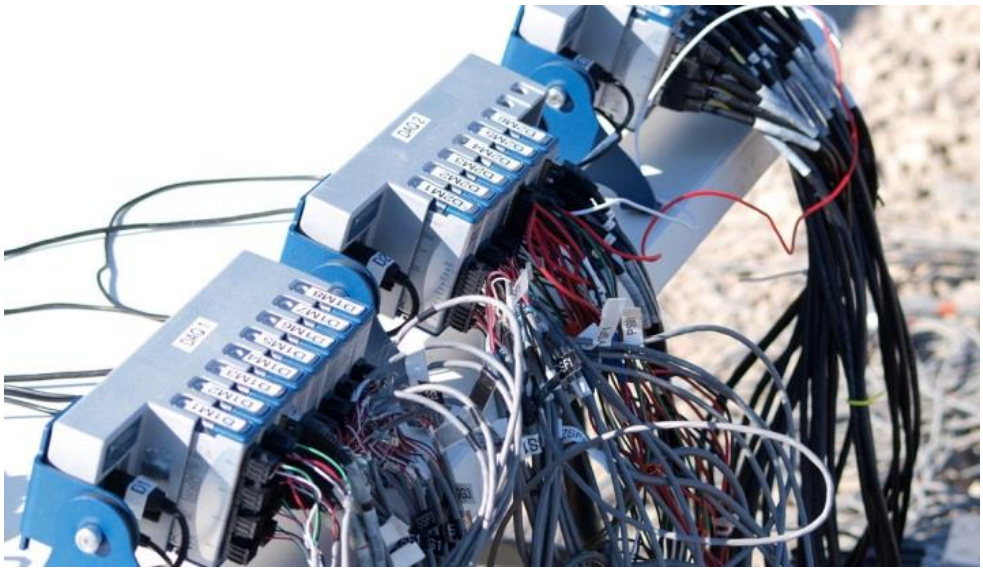

Figure A3: Data acquisition system (Compact DAQ's) fully installed with 120+ channels.

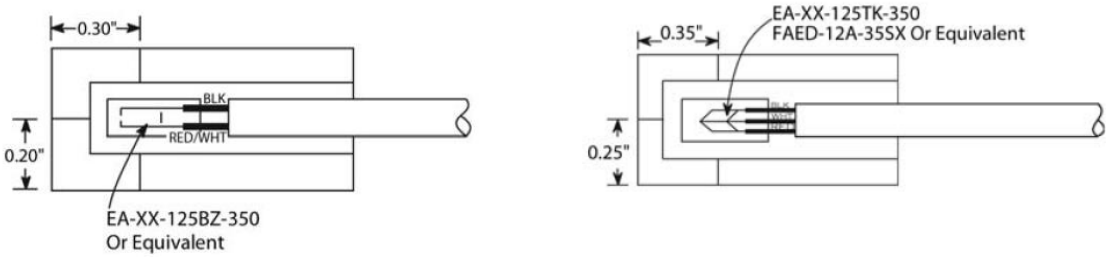

Figure A4: Weldable strain gages: axial (left) and shear (right).

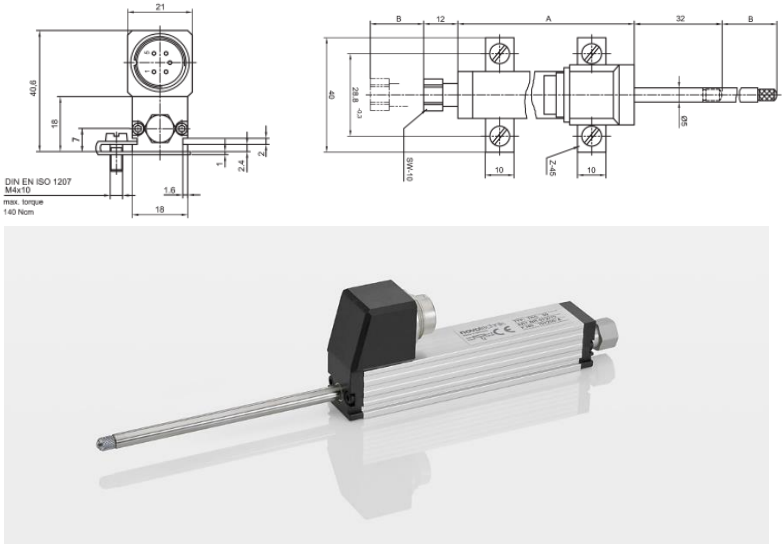

Figure A5: TRS-25 linear potentiometers dimensions (top) and rendering (bottom).

APPENDIX B: TEST PROGRAM

Table B1: List of train passes in test program.

Section*	Consist	Speed (mph)	Runs
RTT	Passenger	15	3
RTT	Passenger	30	3
RTT	Passenger	50	1
RTT	Passenger	60	2
RTT	Passenger	80	3
RTT	Passenger	90	3
RTT	Passenger	102	3
RTT	Freight	2	1
RTT	Freight	15	3
RTT	Freight	30	3
RTT	Freight	38	1
RTT	Freight	41	2
RTT	Freight	60	3
HTL	Passenger	2	1
HTL	Passenger	15	3
HTL	Passenger	30	3
HTL	Passenger	41	2
HTL	Passenger	45	3
HTL	Freight	2	1
HTL	Freight	15	3
HTL	Freight	30	3
HTL	Freight	41	2
HTL	Freight	45	3

*RTT-tangent track; HTL=curved track

Table B2: Static loading test program (using Track Loading Vehicle).

Section	Location	Vertical Load*	Lateral Load*
RTT	Tie C/S	20 kips	10 kips
RTT	Crib D/T	5 kips	2 kips
RTT	Tie E/U	20 kips	10 kips
RTT	Crib F/V	5 kips	2 kips
RTT	Tie G/W	20 kips	10 kips
HTL	Tie C/S	20 kips	10 kips
HTL	Crib D/T	5 kips	2 kips
HTL	Tie E/U	5 kips	2 kips
HTL	Crib F/V	5 kips	2 kips
HTL	Tie G/W	5 kips	2 kips
HTL	Tie H/Y	5 kips	2 kips

* "Loads" represent load steps to maximum of 40kip vertical and 20kip lateral load.

APPENDIX C: DATA ARCHIVE

SOFTWARE:

The data analysis was conducted using National Instruments DIADEM, Microsoft Excel, and MATLAB. DIADEM was used primarily for post-processing and data viewing. Excel was used primarily for data visualization and presentation. MATLAB was used for additional post-processing and calibration.

FILES:

Current data files are in two primary types: LVM and XLSX. LVM files are LabVIEW import files (tab-delineated text files), which contain all of the raw data from the test program. XLSX are Excel spreadsheet files, which contain some of the post-processed data in a variety of formats. The most common spreadsheets contain peak values (max/min) recorded from train passes. The filenames and descriptions of the data to date are shown below in Table and Table .

Table C1: Excel spreadsheet (XLSX) filenames and descriptions.

Filename	Description
RTT_Passenger	Max/min peaks of all channels from each speed of a passenger consist on the RTT (tangent).
RTT_Freight	Max/min peaks of all channels from each speed of a freight consist on the RTT (tangent).
RTT_Passenger	Max/min peaks of all channels from each speed of a passenger consist on the HTL (curve).
RTT_Freight	Max/min peaks of all channels from each speed of a freight consist on the HTL (curve).
Clip_Strain	Clip strains measured from selected runs.
Vertical_Loads	Collection of dynamic vertical wheel loads as measured on the RTT (tangent) and HTL (curve).
Lateral_Loads	Collection of dynamic lateral wheel loads as measured on the RTT (tangent) and HTL (curve).
Rail_Seat_Loads	Collection of dynamic rail seat loads as measured on the RTT (tangent) and HTL (curve).
Vertical_Strain	Collection of static vertical rail web strains as measured on the RTT (tangent) and HTL (curve).
Global_Displacements	Collection of dynamic and static vertical crosstie deflections as measured on the RTT (tangent) and HTL (curve).

Table C2: LVM file names and descriptions of raw data.

Filename	Description	Filename	Description
RTT_65	Passenger 15 mph	HTL_113	no load
RTT_66	Passenger reverse over section	HTL_114	Passenger 2 mph
RTT_67	Passenger 15 mph	HTL_115	Passenger reverse over section
RTT_68	Passenger reverse over section	HTL_116	Passenger 15 mph
RTT_69	Passenger 15 mph	HTL_117	Passenger reverse over section
RTT_70	Passenger 30 mph	HTL_118	Passenger 15 mph
RTT_71	Passenger reverse over section	HTL_119	Passenger reverse over section
RTT_72	Passenger 30 mph	HTL_120	Passenger 15 mph
RTT_73	Passenger reverse over section	HTL_121	Passenger reverse over section
RTT_74	Passenger 30 mph	HTL_122	Passenger 30 mph
RTT_75	Passenger 50 mph	HTL_123	Passenger 30 mph
RTT_76	Passenger reverse over section	HTL_124	Passenger 30 mph
RTT_77	Passenger 60 mph	HTL_125	Passenger 45 mph
RTT_78	Passenger 60 mph	HTL_126	Passenger 45 mph
RTT_79	Passenger 102 mph	HTL_127	Passenger 45 mph
RTT_80	Passenger 102 mph	HTL_128	Passenger 41 mph
RTT_81	Passenger 102 mph	HTL_129	Passenger 41 mph
RTT_82	Passenger 90 mph	HTL_130	no load
RTT_83	Passenger 90 mph	HTL_131	Freight 2 mph
RTT_84	Passenger 90 mph	HTL_132	Freight reverse over section
RTT_85	Passenger 80 mph	HTL_133	Freight 15 mph
RTT_86	Passenger 80 mph	HTL_134	Freight reverse over section
RTT_87	Passenger 80 mph	HTL_135	Freight 15 mph
RTT_88	no load	HTL_136	Freight reverse over section
RTT_89	Freight 2 mph	HTL_137	Freight 15 mph
RTT_90	Freight reverse	HTL_138	Acceleration from stop
RTT_91	Freight 15 mph	HTL_139	Freight 30 mph
RTT_92	Freight reverse	HTL_140	Freight 30 mph
RTT_93	Freight 15 mph	HTL_141	Freight 30 mph
RTT_94	Freight reversal (braking)	HTL_142	Freight 45 mph
RTT_95	Freight 15 mph	HTL_143	Freight 45 mph
RTT_96	Freight reversal (accelerating)	HTL_144	Freight 45 mph
RTT_97	Freight 30 mph	HTL_145	Freight 41 mph
RTT_98	Freight reversal (braking)	HTL_146	Freight 41 mph
RTT_99	Freight 30 mph		
RTT_100	Freight reversal (braking)		
RTT_101	Freight 30 mph		
RTT_102	Freight reverse (25 mph, accelerating)		
RTT_103	Freight 38 mph		
RTT_104	Freight reverse (30 mph, braking)		
RTT_105	Freight 41 mph		
RTT_106	Freight reverse		
RTT_107	Freight 41 mph		
RTT_108	Freight 60 mph		
RTT_109	Freight reverse		
RTT_110	Freight 60 mph		
RTT_111	Freight reversal		
RTT_112	Freight 60 mph		
RTT_113	Acceleration from stop		

APPENDIX D: ADDITIONAL FIELD DATA

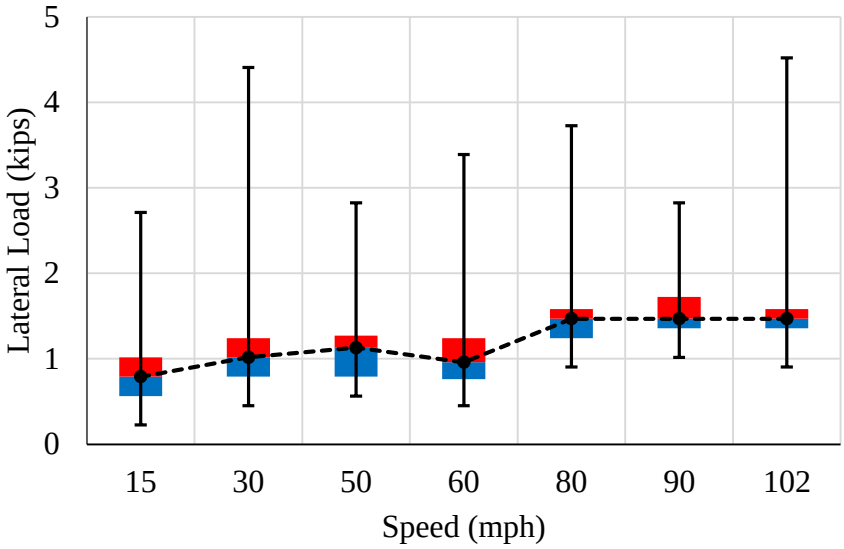

Figure D1: Lateral wheel loads imparted by a passenger consist on tangent track.

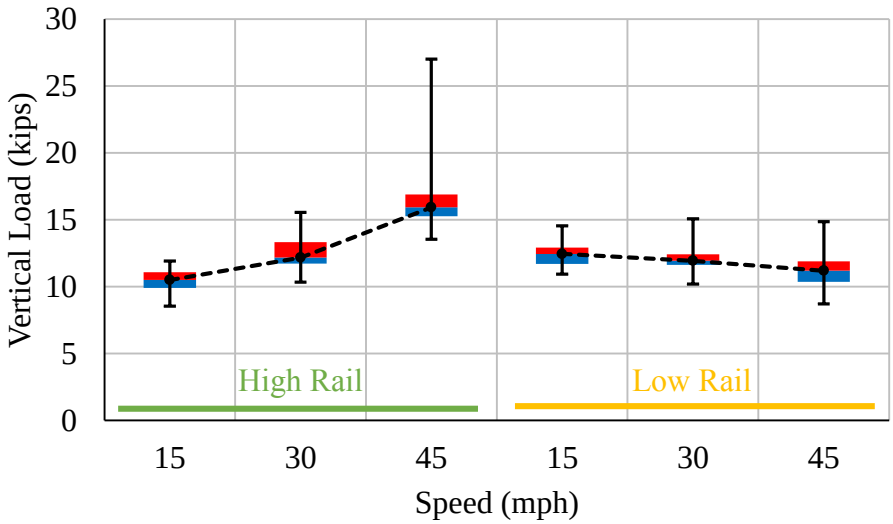

Figure D2: Vertical wheel loads imparted by a passenger consist on curved track.

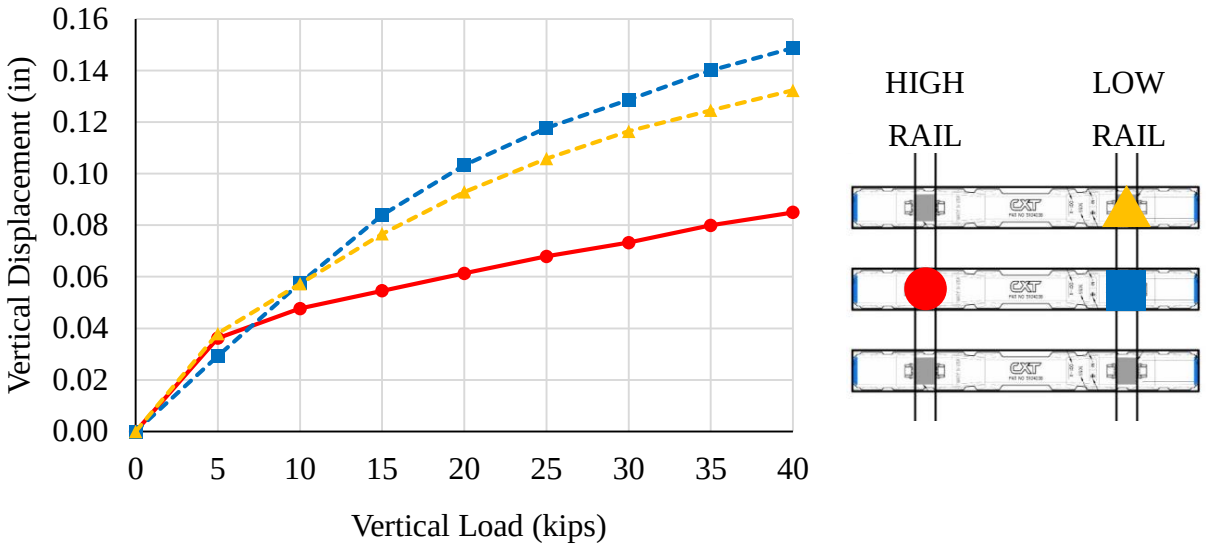

Figure D3: Vertical crosstie displacements and rail seat loads from static vertical loading.

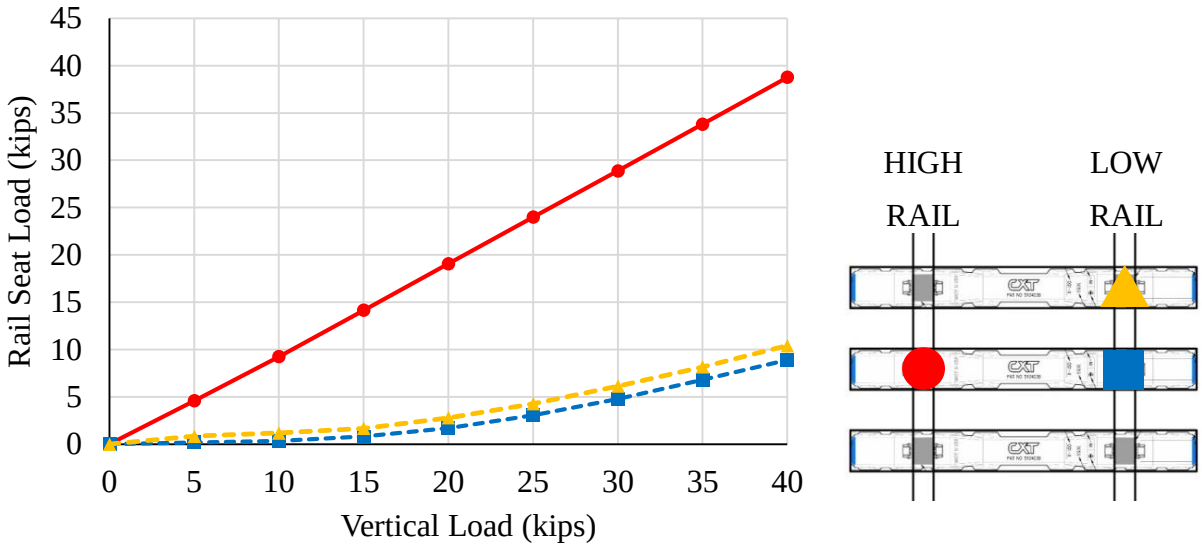

Figure D4: Rail seat loads and associated static wheel loads

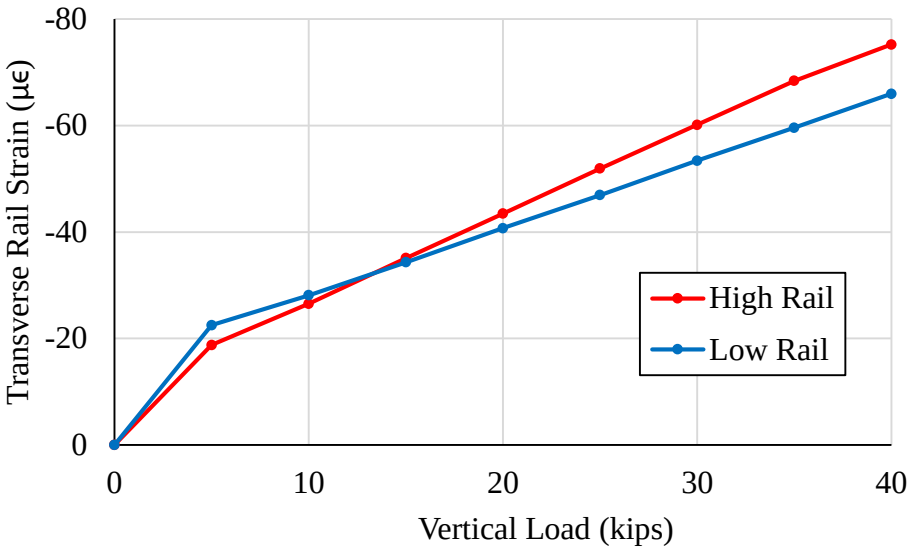

Figure D5: Transverse rail strains with increasing vertical load.

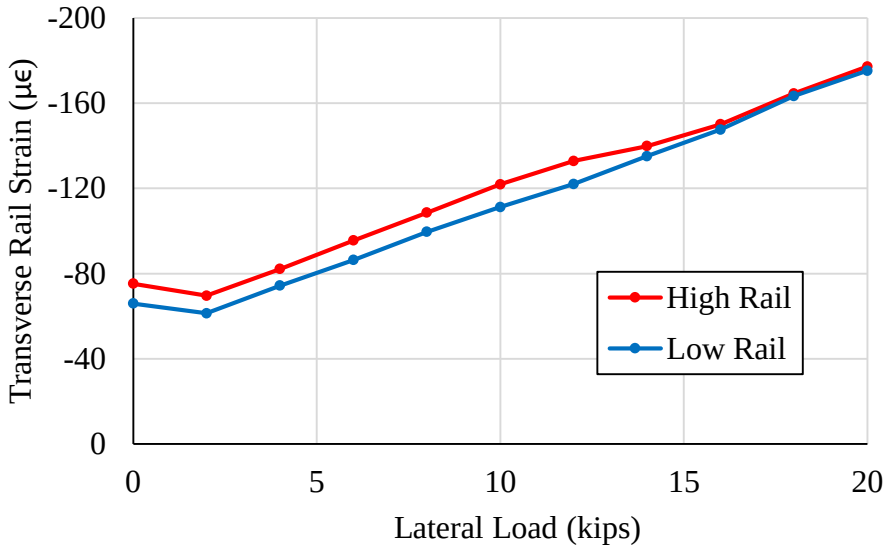

Figure D6: Transverse rail strains with increasing lateral load (and 40kip vertical load).

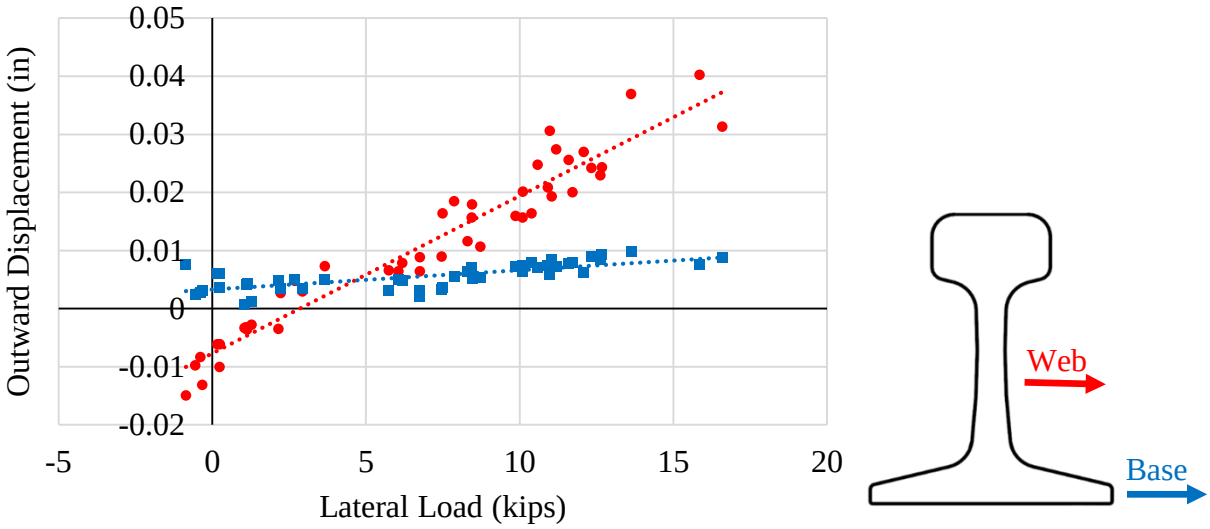

Figure D7: Lateral displacements of the low rail from lateral loads from a freight consist.

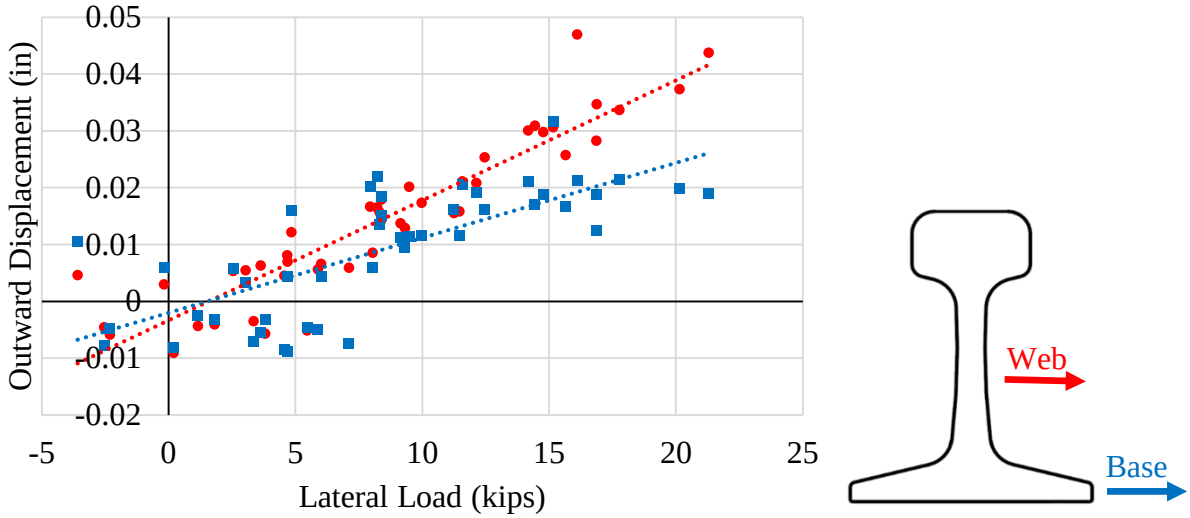

Figure D8: Lateral displacements of the high rail from lateral loads from a freight consist.

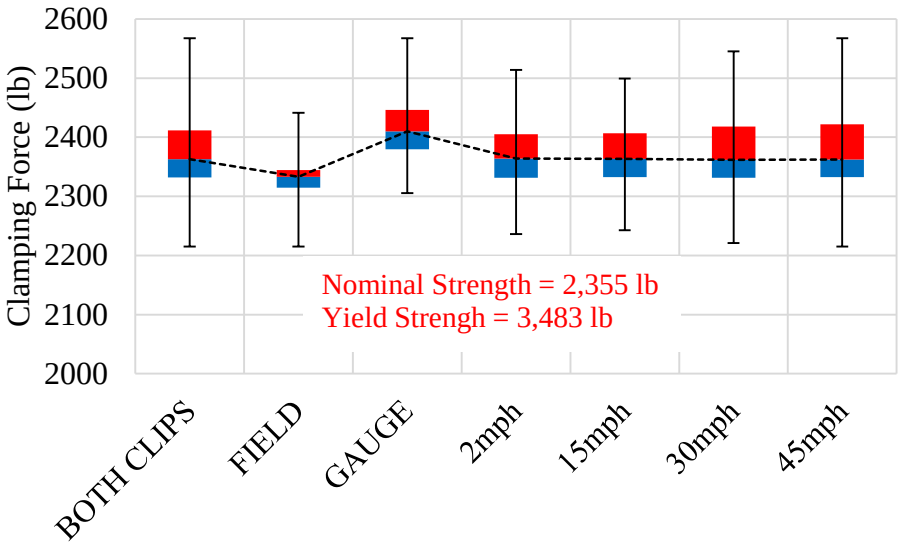

Figure D9: Variability in clamping forces from a freight consist on a curve.

The following Figure D10 and Figure were provided by Christopher Rapp and were presented at the 2013 Joint Rail Conference. Both figures are MBTSS measurements from static TLV loading with a constant vertical force of 40kips.

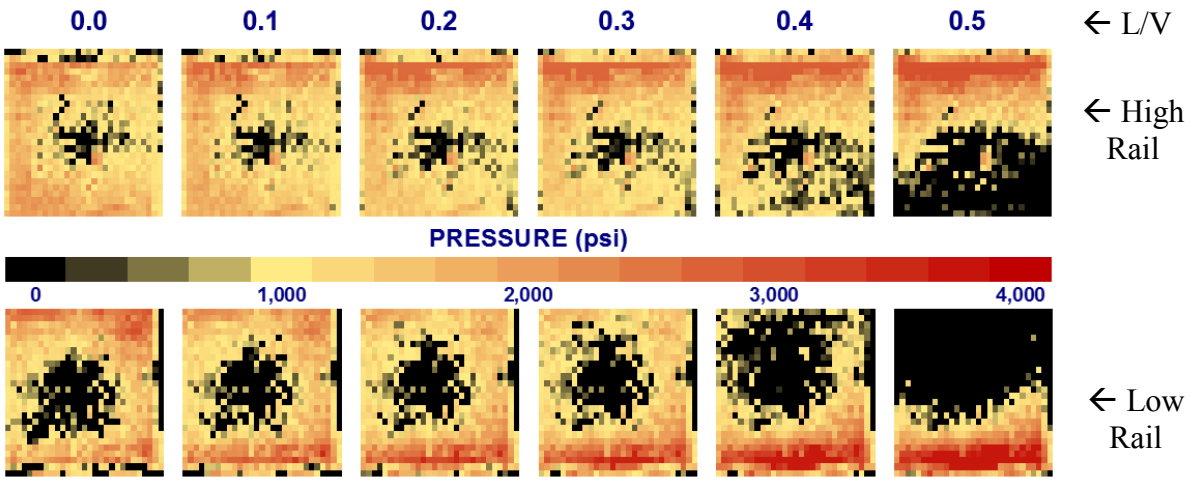

Figure D10: Rail seat pressures at various L/V ratios (top and bottom ends represent field-side)

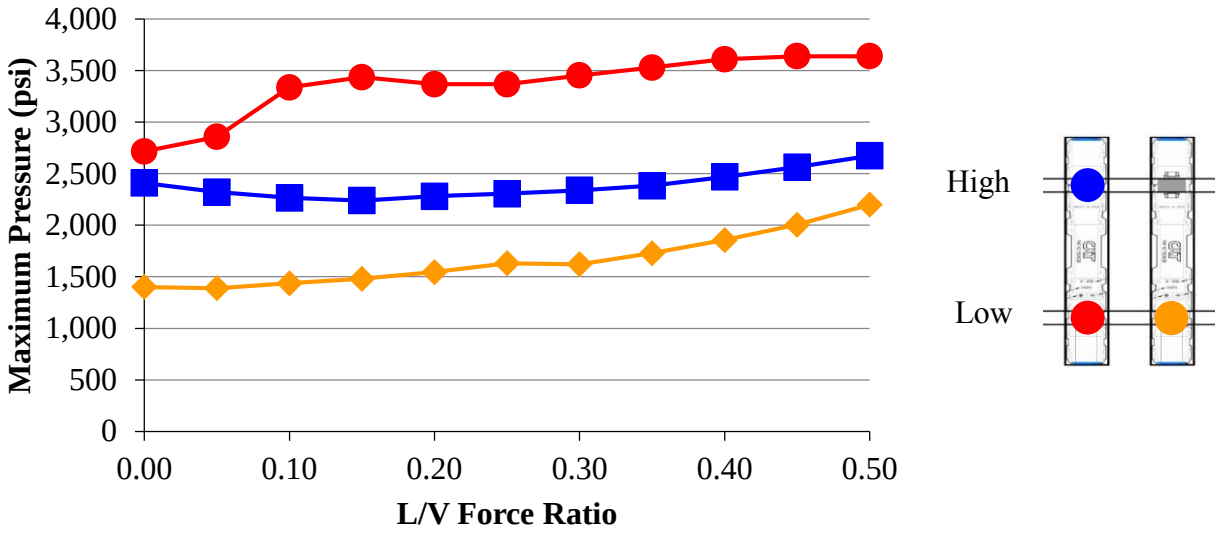

Figure D11: Maximum pressures for various L/V ratios (with vertical load of 40kips)

APPENDIX E: PHOTOS OF FIELD INSTRUMENTATION

Figure E1: Instrumented tangent track section.

Figure E2: Expanded view of fully instrumented rail seats on tangent track.

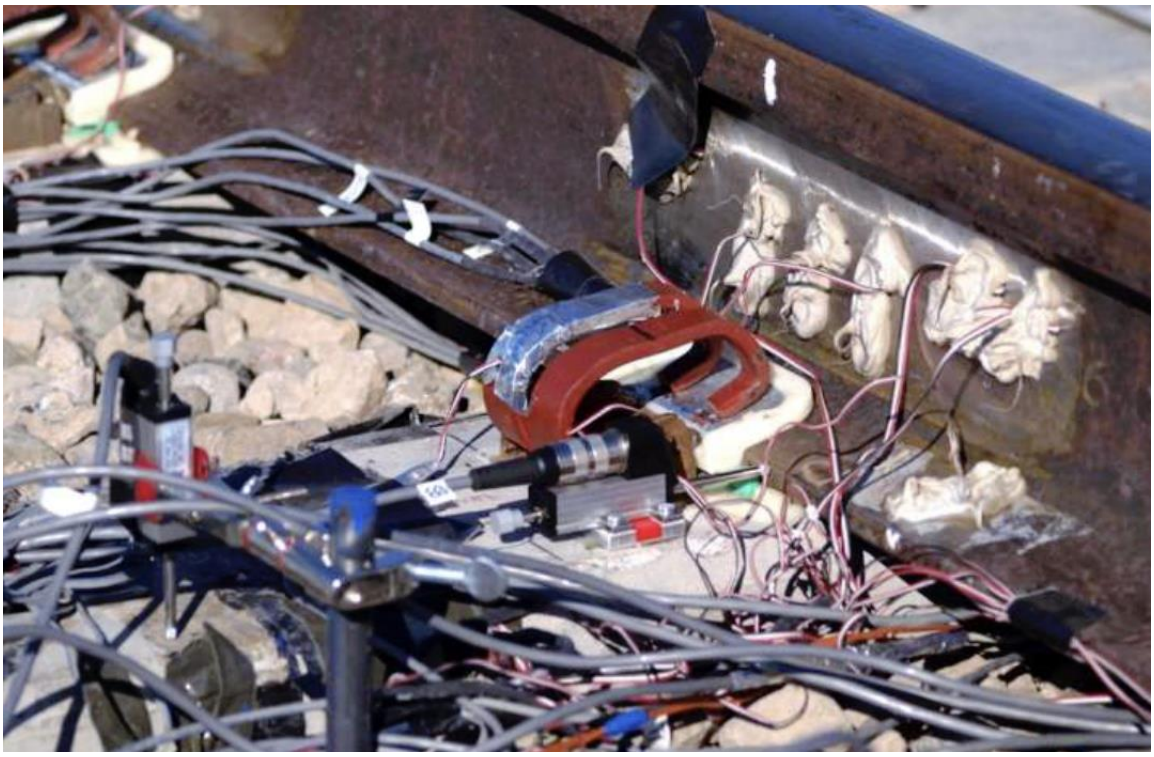

Figure E3: Expanded field-side instrumentation.

Figure E4: Expanded gauge-side instrumentation.

Figure E5: Position of linear potentiometer fixture on the rail (UIUC Lab).

Figure E6: Track Loading Vehicle (TLV).

Figure E7: TLV applying load between fully instrumented rail seats.

Figure E8: Passenger consist operating on tangent track

Figure E9: Freight consist approaching curved track section.

Figure E10: Flat spot on freight car wheel.

Figure E11: Instrumentation setup on the curved track (with freight consist approaching).

Figure E12: UIUC researchers preparing for testing in mobile research lab.

Figure E13: UIUC Concrete Crosstie Research Team in front of the passenger locomotive.

Figure E14: UIUC Concrete Crosstie Research Team on the freight locomotive.

Figure E15: Passenger consist travelling past mobile research lab.